Visible spectroscopic diagnostics: Application and development in fusion plasmas

Sheena Menmuir

Doctoral Thesis

Royal Institute of Technology
Stockholm, Sweden, 2007

Visible spectroscopic diagnostics: Application and development in fusion plasmas

ISBN 978-91-7178-771-2

Doktorsavhandling vid Kungliga Tekniska Högskolan
Fredagen den 7 December 2007, kl 10.00 i FB42 AlbaNova University Center

TRITA-FYS 2007:72
ISSN 0280-316X
ISRN KTH/FYS/--07:72--SE

Atomic and Molecular Physics
Department of Physics
School of Engineering Sciences
Royal Institute of Technology KTH
SE-106 91 Stockholm, Sweden

Abstract

Diagnostic measurements play a vital role in experiments. Without them we would be in the dark with no way of knowing what was happening; of understanding the processes and behaviour occurring; or even of judging the success or failure of our experiments. The development of fusion plasma devices is no different. In this thesis we concentrate on visible spectroscopy based diagnostics: examining the techniques for measurement and analysis; the breadth of plasma parameters that can be extracted from the spectroscopic data; and how the application of these diagnostic techniques gives us a broader picture of the plasma and the events taking place within. Techniques are developed and applied to plasmas in three fusion experiments, EXTRAP T2R, ASDEX Upgrade and JET. The diagnostic techniques exploit different features of the measurements of the emitted photons to obtain various useful plasma parameters.

Determination of the ion temperature and rotation velocity of oxygen impurity ions in the EXTRAP T2R plasma is achieved through measurement and analysis of, respectively, the Doppler broadening and the Doppler wavelength shift of visible wavelength atomic spectral lines. The evolution of the temperature and rotation is studied as a function of the discharge parameters, in particular looking at the effect of applying active feedback control schemes to the resistive wall modes and/or pulsed poloidal current drive. Measurements of multiple ionisation stages are used to estimate radial profiles of the toroidal rotation and the ion temperature and correlations between the ion rotations and the rotation velocities of tearing modes are also established.

Radial profiles of the emissivity and density (or concentration) of the oxygen ions are obtained by means of measurements of the spectral line intensities on a small array of lines-of-sight through the plasma. Changes to the profiles for different plasma schemes and the implications for particle transport are investigated. The derived emissivity profiles are used in the analysis for some of the other spectroscopic diagnostics. Spectral line intensity measurements (in this case of neutral ions) are also the basis for calculations of both the electron temperature and the particle fluxes at the plasma edge. The latter is an indicator of the degree and type of interaction between the plasma and the surrounding surfaces. Particle fluxes of the operating gas hydrogen and of chromium and molybdenum impurities are investigated in EXTRAP T2R for different operating scenarios, in particular changes in the metallic influx with the application of active feedback mode control are examined along with the correspondence between spectroscopic and collector probe results. In the ASDEX Upgrade divertor estimates of the particle flux of the deuterium operating gas are also made through analysis of spectral intensities. Molecular D_2 band structure is explored in addition to the Balmer D_α spectral line intensity to acquire both atomic and molecular particle fluxes, investigate the contribution of the dissociating D_2 to the D_α line and study the effect of changes in the divertor.

Analysis of the D_2 molecular band structure (the relative intensities of the rotational lines and vibrational bands) also enables calculation of the upper state rotational and ground state vibrational temperatures. The locations of emitting atomic ions in JET are estimated from Zeeman splitting analysis of the structure of their spectral lines.

The measurement and analysis of visible wavelength light is demonstrated to be a sensitive diagnostic tool in the quest for increased knowledge about fusion plasmas and their operating scenarios.

Keywords/descriptors: visible spectroscopy, fusion, Doppler shift, Doppler broadening, rotation, ion temperature, particle flux, EXTRAP T2R, ASDEX Upgrade, JET, active feedback mode control, emission profiles, PPCD

Contents

List of publications

This thesis is based on the work presented in the following papers:

I : **S Menmuir**, M Kuldkepp and E Rachlew
Impurity identifications, concentrations and particle fluxes from spectral measurements of the EXTRAP T2R plasma, *Physica Scripta*, **74** (2006) 439-448

II : **S Menmuir**, H Bergsåker, E Rachlew, PR Brunsell, L Frassinetti and JR Drake
Particle flux and surface interaction in EXTRAP T2R, *Proc. 34th European Physical Society Conf. on Plasma Physics, Warsaw* (2007) P1.046

III : **S Menmuir**, E Rachlew, U Fantz, R Pugno, R Dux and the ASDEX Upgrade team
Molecular contribution to the D_α emission in the divertor of the ASDEX Upgrade experiment, *J. Quant. Spect. Rad. Trans.*, **105** (2007) 425-437

IV : M Cecconello, **S Menmuir**, PR Brunsell and M Kuldkepp
Rotation in a reversed field pinch with active feedback stabilization of resistive wall modes, *Plasma Phys. Control. Fusion*, **48** (2006) 1311-1331

V : **S Menmuir**, A Hedqvist, M Kuldkepp, E Rachlew, PR Brunsell, L Frassinetti and JR Drake
Large periodic fluctuations of plasma signals in EXTRAP T2R, *Proc. 34th European Physical Society Conf. on Plasma Physics, Warsaw* (2007) P5.139

VI : PR Brunsell, M Kuldkepp, **S Menmuir**, M Cecconello, A Hedqvist, D Yadikin, JR Drake and E Rachlew
Reversed field pinch operation with intelligent shell feedback control in EXTRAP T2R, *Nuclear Fusion*, **46** (2006) 904-913

VII : M Cecconello, M Kuldkepp, **S Menmuir**, A Hedqvist and PR Brunsell
Current profile modifications with active feedback stabilization of resistive wall modes in a reversed field pinch, *Proc. 33rd European Physical Society Conf. on Plasma Physics, Rome* (2006) P4.149

VIII : M Kuldkepp, PR Brunsell, M Cecconello, R Dux, **S Menmuir** and E Rachlew
Measurements and modelling of transport and impurity profiles in the EXTRAP T2R reversed field pinch, *Phys. Plasmas*, **13** (2006) 092506-1-8

IX : M Kuldkepp, PR Brunsell, JR Drake, **S Menmuir** and E Rachlew
Method for measuring radial impurity emission profiles using correlations of line integrated signals, *Rev. Sci. Instrum.*, **77** (2006) 043508-1-6

In papers I, II and III, I was responsible for the spectroscopic measurements, for the calibration procedures and for the analysis (including line identifications and determination of ion concentrations, T_e, particle fluxes and molecular temperatures) and also for writing the paper (with discussions from the co-authors, who also had analysis input in paper III).
I was responsible for the spectroscopic measurements and subsequent analysis in paper IV, took part in discussion and wrote parts of the paper.
In paper V I took part in the experiment, participated in the analysis, discussion and wrote much of the paper.
In papers VI and VII I was involved in the experiments and was responsible for spectroscopic measurements and ion velocity and temperature analysis, I participated in the discussion and in writing selected parts of the paper.
In papers VIII and IX, I was involved in the experiments and discussion.

Other publications related to but not included in this thesis

1. S Günter *et al.* (including S Menmuir), Overview of ASDEX Upgrade results – development of integrated operating scenarios for ITER, *Nucl. Fusion*, **45** (2005) S98

2. H Bergsåker, S Menmuir, E Rachlew, PR Brunsell, L Frassinetti and JR Drake, Metal impurity fluxes and plasma-surface interactions in EXTRAP T2R, *Journal of Physics: Conference Series*, **(***17th International Vacuum Congress, Stockholm* 2007)

3. K Krieger M Stamp, S Brezinsek, HG Esser, S Jachmich, A Kreter, S Menmuir, Ph Mertens, V Philipps, P Sundelin and JET EFDA contributors, Evolution of Be migration after Be evaporation in the JET tokamak, *Proc. 34th European Physical Society Conf. on Plasma Physics, Warsaw* (2007) P1.041

4. PR Brunsell, D Yadikin, D Gregoratto, R Paccagnella, YQ Liu, T Bolzonella, M Cecconello, JR Drake, M Kuldkepp, G Manduchi, G Marchiori, L Marrelli, P Martin, S Menmuir, S Ortolani, E Rachlew, G Spizzo and P Zanca, Active control of multiple resistive wall modes, *Plasma Phys. Control. Fusion* **47** (2005) B25

5. S Menmuir, M Cecconello, M Kuldkepp, E Rachlew, PR Brunsell and JR Drake, Ion and mode rotation in the EXTRAP T2R device during discharges with and without the application of feedback control, *Proc. 32nd European Physical Society Conf. on Plasma Physics, Tarragona* (2005) P4.079

6. PR Brunsell, E Olofsson, L Frassinetti, S Menmuir, M Cecconello, D Yadikin, M Kuldkepp, JR Drake and E Rachlew, Resistive wall mode feedback control experiments in EXTRAP T2R, *Proc. 34th European Physical Society Conf. on Plasma Physics, Warsaw* (2007) P1.103

7. L Frassinetti, PR Brunsell, JR Drake, S Menmuir and M Cecconello, Spontaneous QSH in the EXTRAP T2R reversed-field pinch, *Proc. 34th European Physical Society Conf. on Plasma Physics, Warsaw* (2007) P1.115

8. L Frassinetti, PR Brunsell, JR Drake, S Menmuir and M Cecconello, Spontaneous Quasi-Single Helicity regimes in EXTRAP T2R reversed-field pinch, *accepted by Phys. Plasmas*, (2007)

9. G Vall-llosera, J Álvarez Ruiz, P Erman, E Melero García, E Rachlew, S Menmuir and M Stankiewicz, The npσ,π to EF emission systems in D_2 studied by selective excitation, *J. Phys. B: At. Mol. Opt. Phys.*, **38** (2005) 659

10. E Melero García, J Álvarez Ruiz, S Menmuir, E Rachlew, P Erman, A Kivimäki, M Glass-Maujean, R Richter and M Coreno, Fluorescence study of doubly excited states of molecular hydrogen, *J. Phys. B: At. Mol. Opt. Phys.*, **39** (2006) 205

1. Introduction

This thesis will demonstrate some of the applications of visible spectroscopy in fusion experiments and its suitability as a sensitive diagnostic tool by taking examples from various projects. Specifically, it will show spectroscopy in action in three different devices: a medium sized reversed field pinch; a medium tokamak; and a large tokamak. The fusion plasmas in the three devices are very different and have their own issues and challenges and, as a consequence, although some spectroscopic applications are universal or appear in different guises, some are more specific. The strength of spectroscopy is the information about the plasma, the applied schemes and scenarios that it can provide and the visible spectroscopic results herein are discussed in this context. Another aspect that reoccurs in this thesis is the comparison of spectroscopic results with those obtained by other measurement techniques, the agreement between which demonstrates the viability of the spectroscopic based techniques.

The field of plasma spectroscopy is well established and there exist several comprehensive reviews and detailed sources for reference [1-7]. As the visible light from the plasma can be transported via fibre optics to the detector location, no direct connection between the vessel and detection system is needed for visible spectroscopy. This added flexibility of visible spectroscopy over other aspects of photon spectroscopy means that the development of visible spectroscopic diagnostic techniques in plasmas is well advanced.

I would like to begin by giving a brief introduction into the world of fusion, visible spectroscopy and into the three experiments included here. In section 2 I will then introduce some of the concepts and techniques related to spectroscopy in fusion. The methods and some of the associated issues and necessary assumptions and simplifications will also be discussed. The focus will be on the spectroscopic diagnostic techniques applied in this thesis. Section 3 will then include some discussion and examples of spatial profiling something that has implications in many areas of this research. Much of my work has been connected with control and confinement in fusion plasma experiments and so I shall say a few words about this in section 4. I will also explore some of the other areas in which I have applied spectroscopy including the study of particle fluxes. Section 5 will be a summary of the papers included in this thesis before I finish with section 6 and some conclusions and outlook for the future. An explanation of the abbreviations and symbols used in the text is included at the end.

1.1 Fusion, confinement, diagnostics and spectroscopy

The fusion reaction involves fusing two nuclei to form a heavier nucleus with the release of energy. This reaction is the basis for stellar (solar) energy where progressively heavier

elements undergo fusion as the star ages. To be able to harness this power on Earth could prove invaluable in the future when the need for diversification in and replacement of our current energy sources becomes even more critical than it is today.

On Earth fusion reactions between hydrogen isotopes are favourable as the mutual repulsion of the nuclei can be overcome at lower plasma temperatures than for other reactants [8]. The conditions required for fusion to take place are still extreme and a hot plasma environment is required (giving the nuclei enough thermal energy to overcome their mutual repulsion and undergo fusion). Such a plasma needs to be confined and one promising confinement method is through the use of magnetic fields, where the charged particles gyrate around the field lines and travel long distances in the plasma parallel to the magnetic field before escaping (the magnetic field balances the plasma pressure) [9]. An alternative confinement technique is inertial confinement where small targets are heated and compressed in order to initiate the fusion reaction. There is a wide body of research in this field, for example described in [10], however such experiments are not the subject of this thesis.

Confinement of the plasma particles, in particular the length of time they can be contained within the plasma (the particle confinement time), is a key parameter for the success of fusion devices. The particles must be able to react before they lose their energy or escape and the fusion produced α-particles should have time to pass on their energy to the plasma. A dense plasma is also critical. There must be a power balance within the plasma with the power input (from ohmic and external heating) and self-heating provided by the energy rich α-particles balancing losses from the radiated power. 'Ignition' is reached when the self-heating alone is sufficient to balance the losses. For power production in future reactors it is necessary that more power be produced, and collected, than is put in. It is foreseen that the energetic neutrons produced in deuterium-tritium fusion reactions will be the primary source of the extracted energy.

Impurity influx is an important issue in fusion plasmas since it can have a significant effect on the plasma, its performance and indeed its ability to sustain fusion. The impurities lead to increased radiation losses and are also a powerful source of electrons leading to a dilution of the plasma density. A plasma of 2% oxygen or of 0.7% iron will increase the electron density by about 15% [11]. Too high a concentration of impurities, in particular of high-Z materials, can lead to discharge termination. Control of the levels of the fusion-produced α-particles is also important [12].

Within magnetic confinement there are different arrangements of the magnetic field lines, of which the tokamak, reversed field pinch (RFP) and the stellarator are the most studied. The plasma is confined within a torus vessel whose cross-section depends on the confinement configuration. In the RFP [13, 14] the poloidal and toroidal components of the confining helical field are of a similar magnitude, being produced respectively by a toroidal current in the plasma (induced by a transformer) and by the plasma itself via a dynamo process. A reversal in the toroidal field direction near the edge with respect to the centre gives rise to the name. In contrast, in a tokamak device [15] the toroidal component is produced by external current carrying poloidal loops and is greater than the poloidal component (typically by a factor of 10).

For the development, and indeed for the success, of any scientific enterprise the need for understanding what is taking place and information on the conditions and interlinked parameters is the key. Diagnostic measurements, analysis and interpretation are important tools in information gathering as an aid to understanding the experiments. All fusion experiments include measurements on a wide range of diagnostic systems. One diagnostic avenue is visible spectroscopy and most of this thesis deals with this approach: diagnosis of plasma parameters via measurements of visible wavelength photons (originating from interaction of the particles and the fields). Knowledge and modelling of the underlying

atomic and molecular processes is central to the analysis. Information about different aspects of the plasma can be obtained from various features of the photons emitted in the plasma. Table 1 summarises the translations between the spectroscopy (atomic/molecular physics) and the plasma parameters highlighted in this thesis.

Spectroscopic aspect	Plasma parameter
Doppler line broadening	Ion temperature T_i
Doppler wavelength shift	Ion rotation velocity v_i
Line or multiplet intensity	Particle flux Γ
Molecular band intensity	Molecular particle flux Γ
Intensity on multiple lines-of-sight	Emissivity profile $\varepsilon_i(r)$
Molecular band structure (relative line intensities)	Rotational and vibrational temperatures T_{rot}, T_{vib}
Zeeman splitting	Local magnetic field B or ion emission position (if B distribution is known)
Line intensity ratios	Local electron temperature T_e and/or density n_e
Integration over full vacuum ultraviolet (VUV) spectrum	Radiated power P_{rad}
$\varepsilon_i(r)$ with $T_e(r)$ and $n_e(r)$	Ion density profile $n_i(r)$ or ion concentration n_i/n_e

Table 1: Examples of measured spectroscopic features and the corresponding plasma parameters that can be obtained.

The development of fusion as a viable commercial power source continues with the construction of the next stage experimental device ITER [16]. The device, figure 1, will be located in Cadarache, France. It is an international collaboration with seven partners (at the time of writing) – the European Union, Japan, Peoples' Republic of China, Russian Federation, the United States of America, the Republic of Korea and India. A step-up in terms of physical size and capabilities including superconducting magnets and remote handling, the obtainable plasma parameters will be much closer to those of a fusion reactor and the experiment will be a valuable test bed of current scaling laws, predictions and design details (including wall materials and control schemes). A wide range of diagnostic devices are planned to study all areas of the plasma – core, edge, divertor and scrape-off layer (SOL). [17].

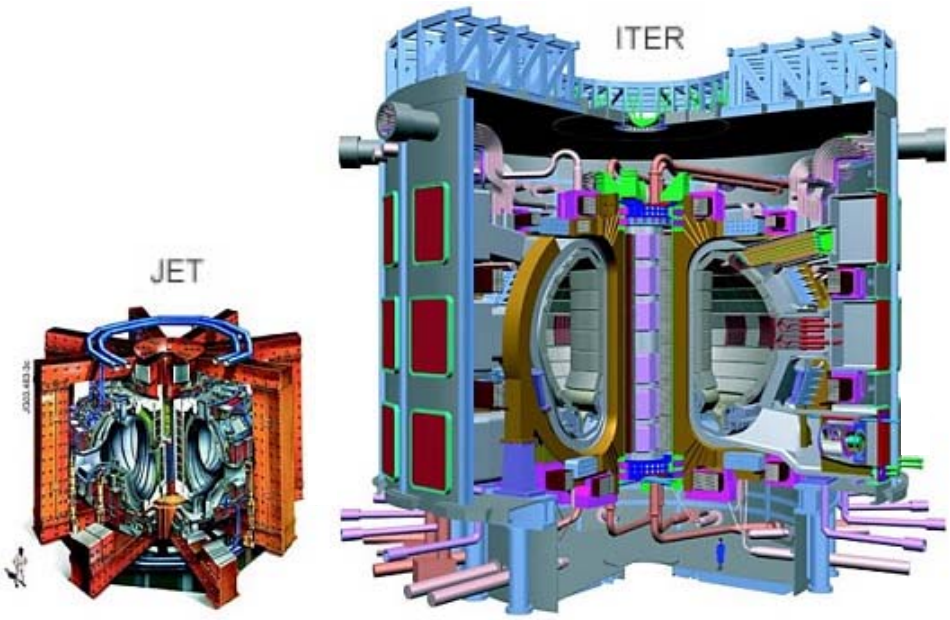

Figure 1: Cut-away diagram of the ITER device (right). Also shown is the JET device (left) for comparative purposes. Both diagrams include a 'standard man' for size perspective [18].

1.2 EXTRAP T2R

EXTRAP T2R is a reversed field pinch device in Stockholm, Sweden (Alfvén laboratory in KTH) [19, 20]. It is a medium sized RPF with a major radius (R_o) of 1.24m and minor plasma radius (a) of 0.183m, a stainless steel vessel and molybdenum mushroom limiters – the latter with 8% surface coverage. There is no carbon in the plasma facing components apart from the small fraction present in the stainless steel. Typical operating parameters are: a hydrogen plasma; plasma current (I_p) of 75-140kA; line averaged electron density $\langle n_e \rangle \sim 10^{13} cm^{-3}$; reversal parameter F in the range –0.8 to –0.1 and pinch parameter θ of 2.8 to 1.4. Development of an active feedback control system for the suppression of resistive wall mode growth is central to the EXTRAP T2R program. With applied feedback control the discharge length has been prolonged from ~15ms to up to more than ~80ms, which is more than 10 wall times (penetration time of the vertical magnetic field) [paper VI].

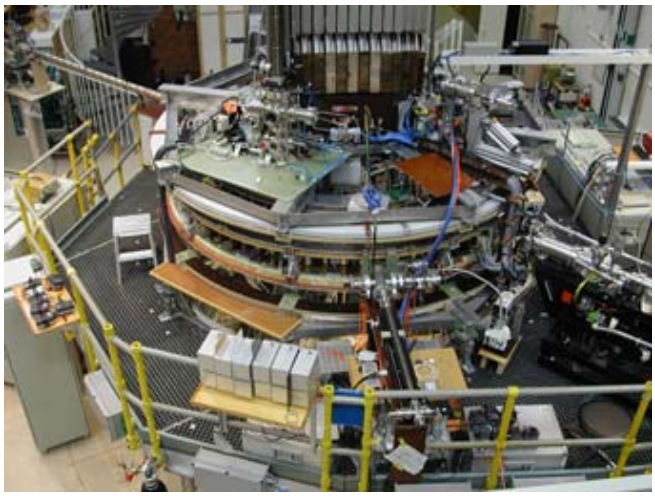

Figure 2: The EXTRAP T2R experiment [19]. The main structure in the centre back of the figure is the ion core.

The loop sensors that form part of the feedback system also act as the measurement system for the magnetic modes (including amplitude and angular phase velocity). There is a two-colour interferometer (HeNe and CO_2) for the line-averaged electron density and a Thomson scattering system for on-axis electron temperature measurement. Collector probes (and electrostatic probes) can be inserted into the plasma edge. There is also a bolometer system with an eight-chord array and gold film detectors sensitive in the ultraviolet (UV) to soft x-ray (SXR) range.

There are a variety of spectroscopic diagnostic systems on EXTRAP T2R including a SXR array (with filters and SXR sensitive detectors) and vacuum ultraviolet (VUV) spectrometer (10-120nm). There are photo-multiplier tube (PMT) detectors with hydrogen Balmer-α (H_α) filters (width 1nm), and two visible wavelength monochromators – 25cm focal length Ebert type and 27.5cm focal length crossed Czerny-Turner type – with PMT detectors and fast temporal response. There is a half metre Ebert monochromator with visible wavelength radiation collected from five fibres (a poloidal array of lines-of-sight) and measured by individual PMT detectors [21]. Additional half metre Ebert and one metre Czerny-Turner spectrometers with optical multi-channel analyser (OMA) detector systems can measure the time resolved spectrum. The two spectrometers measure windows of up to approximately 30nm and 10nm respectively. It is possible to vary the width and delay of the time interval in which the light is collected. By recording only a portion of the total available pixels multiple scans are possible within a single discharge. The toroidal positions of the visible spectroscopy diagnostics can be varied as the light is transmitted from the vessel ports to the diagnostic instruments by fibre optics. Figure 3 shows the diagnostic toroidal positions including the typical locations for the visible spectroscopy. The number of diagnostic ports is limited in order to preserve the resistive shell. The spectroscopic diagnostics are an integral part of the full program.

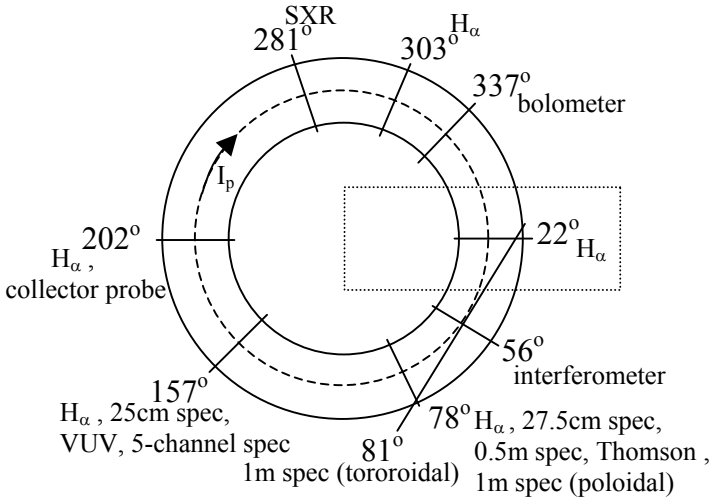

Figure 3: Schematic diagram of EXTRAP T2R top-view showing an example of the toroidal positions of spectroscopic diagnostics and the direction of the plasma current. The dotted rectangle represents the iron core. At many of the toroidal locations there are both horizontal and vertical lines-of-sight.

1.3 ASDEX Upgrade and JET

ASDEX Upgrade in Garching, Germany and JET in Culham (Oxfordshire), England are both tokamak experiments.

The German experiment [22-24] is part of the Max-Planck Institute for Plasma Physics. It has a major radius of 1.65m and minor radii of 0.8m (vertical) and 0.5m (horizontal). The typical working gas is deuterium and discharges are of the order of 8sec. The machine has a divertor configuration with tungsten and carbon tiles for the plasma facing components. One major element of the ASDEX Upgrade mission is in the experimental development of the plasma facing components and gradually the machine has been converted to a fully tungsten device. During the experiments described herein the walls were a mixture of carbon and tungsten with an all carbon divertor.

There are a range of standard diagnostics on ASDEX Upgrade and a good selection of possible lines-of-sight for spectroscopic use including several arrays in the divertor. The studies included in this thesis concentrate on spectroscopy in the divertor region, in particular the outer divertor, and the divertor properties. Three different high resolution spectrometers, of both Czerny-Turner and Echelle design with charge-coupled device (CCD) detectors, are used in these studies.

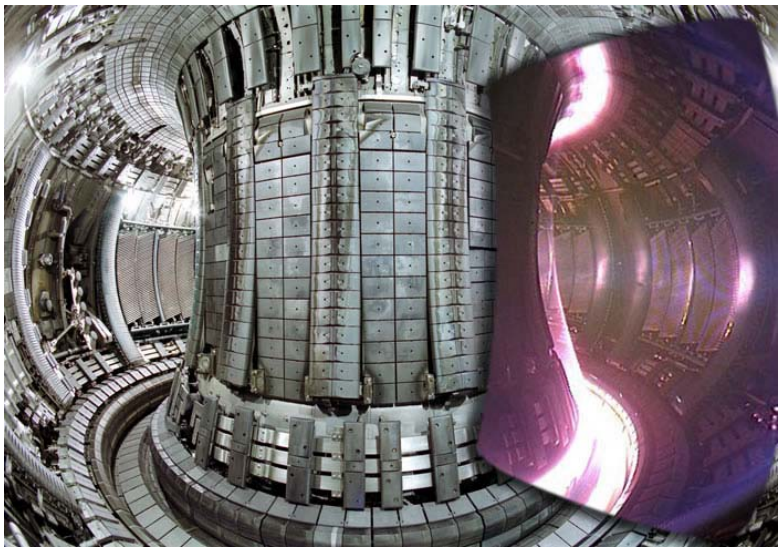

Figure 4: The inside of the JET tokamak (2005): (left) without plasma and (right) with plasma (in infra-red) [18]. The D-shaped plasma cross-section and divertor structure at the bottom of the tokamak, where the light is most intense, can be clearly seen.

The JET tokamak (figure 4) is a European (EFDA) collaboration [18] with researchers participating from all over the world. It is a large tokamak (currently the largest in the world) with a major radius of 2.96m and minor plasma radii of approximately 2.10m (vertical) and 1.25m (horizontal). It has a divertor configuration and operates mostly in deuterium with a typical current flat-top length of 10s of seconds and on-axis magnetic field up to ~4T. Various current drive and heating systems are installed and there is a wide range of diagnostic capabilities including a number of spectroscopic tools. The current focus is towards issues for ITER including the development of steady-state operating scenarios and study of, for example, instabilities and transport.

2. Spectroscopic diagnostics (techniques, assumptions, limitations)

From its most basic, identifying the (radiating) constituents in a plasma, to complex analysis involving transport codes and atomic processes, spectroscopy or the detection of photons emitted by the plasma, is a skilful and practical tool in the diagnosis of fusion plasmas.

Here, we concentrate on passive spectroscopy where no direct effects are felt by the plasma as a consequence of the measurement. This is one of the primary advantages with this type of detection, it is non-invasive, non-disturbing and does not require special plasma scenarios. This relative simplicity makes it suitable for measurements on simpler devices (without neutral beams, external heating sources, crossing arrays of multiple lines-of-sight etc.) or in divertor regions of larger machines. Other spectroscopic techniques can be more invasive as they require, for example, interaction with the ions in an injected neutral beam in order to produce the emitted radiation profiles.

Detection of photons emitted by a fusion plasma has a wide range of possible interesting and useful applications. A key factor is the analysis of the observed spectra that through applying different techniques relates the atomic (or molecular) physics of the observed data with corresponding plasma parameters, extracting diagnostic information (see Table 1 for examples). This chapter will introduce a few of the many varied techniques utilised in spectroscopic diagnostics of fusion plasmas, focussing on the methods exploited and developed in this thesis. It will also discuss some of the relevant limitations and assumptions that have been significant in this analysis.

2.1 Calibration

For quantitative spectroscopic measurements calibration is important. Calibration in terms of wavelength is a necessity for all spectroscopic work. It is important for the identification of observed spectral lines and determination of how much they have shifted or are separated. This can be done using emission sources with known wavelengths (such as spectral lamps) or through identifying features in a plasma spectrum, for instance, lines of the Balmer series or a distinctive multiplet belonging to a species present in the plasma. However, if plasma lines are used then care must be taken to avoid instances where the line position might be affected by the measurement geometry, for example where the spectral line might be shifted due to flow of the plasma with respect to the line-of-sight observation. Wavelength calibration has been carried out for all the spectroscopic systems exploited here.

Absolute intensity calibration is useful when the intensity emitted by a particular source (ion or molecule) in the plasma is of interest and also when quantitative determination of changes in emission intensity is desired. This can be extended beyond simple photon counts to, for example, particle or population estimates with applied modelling. The usual method for intensity calibration is to measure the light from a calibration lamp (such as an integrating sphere). It is important to consider the different elements in the measurement system: the vessel windows, transmission fibres, spectrometer, detector and any further amplification or filtering as the number of photons or signal is affected in passing all the stages. Due to the impossibility of having the calibration source inside the EXTRAP T2R vessel the spectroscopic intensity calibrations described in the papers do not include the (quartz) port window that lets the light pass out of the torus. Some cleaning of the windows has occurred during vacuum breaks and in general it is assumed that there is negligible absorption in this element of the transmission path, although some effects have been noted in paper VIII.

Relative calibration can also be useful, either to relate the intensity measured in a combination of calibrated and uncalibrated spectrometers or to relate measurements made in different discharges. The first of these can be accomplished by measuring the same emission with the two systems and is also discussed in section 3.7 and paper III. The latter, done by measuring the same or an overlapping wavelength region, can be a check on the reproducibility of the discharges or an opportunity to measure separate wavelength intervals or a wider wavelength range than possible in a single measurement (see also paper III).

The integrating sphere intensity calibration light source emits a continuum over a wide wavelength range. Similarly, continuum radiation is also emitted by the fusion plasma due to Bremsstrahlung and recombination radiation. This is in addition to the line radiation emitted due to the radiative decay of excited states. For the most part, this work concentrates on measurements of line radiation, both atomic lines or multiplets and molecular band radiation.

In analysing an emission line feature, there are generally several parameters that are of primary interest, including the peak intensity, the wavelength of the peak intensity and the width of the line. A simple way to accurately determine these (and the line features more generally) is to fit the measured spectral region with a single or series of curves. Gaussian, Lorentzian or general line shape curves as in figure 5 are commonly used [25]. Implicit in the use of these functions, however, is the assumption that the line shapes are symmetric. In cases where this does not apply, a combination of more than one curve may be required.

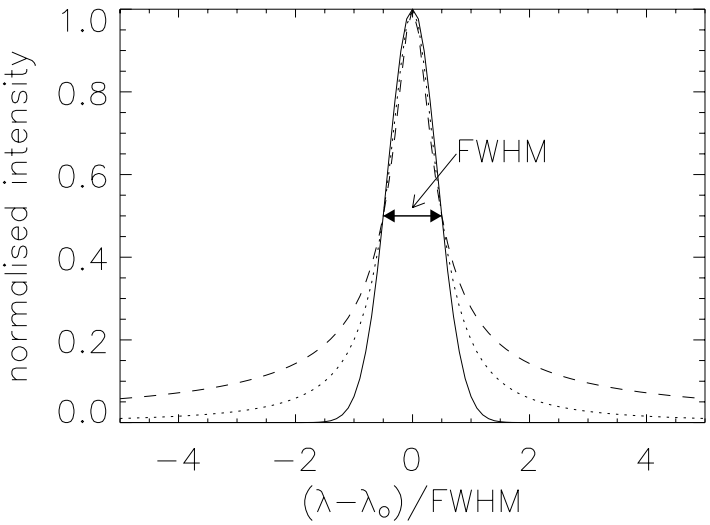

Figure 5: Line shape for Gaussian (——), Lorentzian (·····) and general line shape with maximum tails (– – –) with equal full width at half maximum (FWHM) and peak intensity, calculated from [25].

The accuracy and statistics achievable in order to successfully extract the results is limited by the instrumentation. One limitation is due to the spectral resolution of the system, which defines the degree of detail seen in the spectrum. A higher resolution system enables close lying spectral lines to be discerned separately. This can aid identification in the spectrum (for instance, separating ion lines or showing molecular rotational band structure) and examination of the line shape (for example, showing Zeeman split components or isotopic contributions such as D_α and H_α). The instrumental function determines the resolution of the system and must be included in line width analysis, see section 2.3. One way to determine it is by using the system to measure a source with narrow lines, for example the neutral spectral lines emitted from noble gas spectral lamps. The instrumental function can then be determined by fitting the measured line shape with a suitable curve (such as a Gaussian) and calculating the full width at half maximum (FWHM). If the dispersion changes with wavelength then the instrumental function might also have some wavelength dependence. There is indeed a small variation in the instrumental function of the 1m focal length spectrometer used for the ion temperature measurements in EXTRAP T2R – the measured $FWHM_{Inst}$ is 0.096nm at 278.1nm (OV) and 0.085nm at 441.5nm (OII). In a monochromator or filter system, the instrumental function usually plays a different role as it determines the wavelength window in which the light is collected. For example, with a narrow window, the system can quite easily be used to measure the total intensity of single isolated lines, but with a wider window, close neighbours may be within the wavelength interval and contribute to the measured intensity too. Such line intensity measurements are discussed in more detail in section 2.4.

In general toroidal symmetry has been assumed in these analyses. This assumption enables us to compare measurements taken at different toroidal locations although it is important to be aware of local factors, for example gas puffing in specific locations which can break this symmetry (paper III and also seen in EXTRAP T2R H_α). Often some form of poloidal symmetry is also assumed, in particular in radial profiling. The assumption is generally less valid in those tokamaks where the cross-section is non-uniform.

2.2 Line positions

One of the most basic uses of spectroscopy in fusion plasmas is the identification of the emission sources. Through the wavelengths of the emitted line radiation from atomic ions, and the molecular band emission if present, the constituents of the plasma can be determined. A similar approach is used in the identification of astrophysical species in the stars and interstellar material [26] where further analysis involving the line intensities and shifts yields additional information.

In using a survey scan to identify the constituents of a plasma through the identification of the observed emission lines as in paper I, there are considerations about the measurements and the sources that can be useful to aid the process. In terms of the measurement it is useful to consider the line-of-sight for the photon collection – there will likely be differences if looking through the whole plasma (with a line-of-sight that traverses the edge and core) or just through the edge or in the divertor. Also to be considered is, given the local conditions (such as electron temperature) what ionisation stages are possible or likely and whether the conditions are right for molecules – are the observations made in the divertor rather than in the main plasma? The environment (plasma and the surroundings) should be considered in terms of the possible sources and most likely elements. It is easiest to start with distinctive features (such as the CrI triplets in our EXTRAP T2R plasma) or molecular band structure (such as the CD Gerö band $A\ ^2\Delta - X\ ^2\Pi$ [27]) and known strong or persistent lines of the

suspected ions – using sources of emission line information such as [28, 29]. Remember, if there is one line of a multiplet then all the components (at least those of reasonable intensity) can also be expected, if one or more are missing then is this the right identification?

The shift in wavelength of an observed emission line from its known (theoretical) position is also a common useful tool in diagnostics. In fusion it can provide information on rotation and the movement of ions in the plasma. This technique of measuring Doppler shifts has also been used in the discovery of new extrasolar planets (exoplanets) [30, 31]. The Doppler shift relationship between the velocity v of the emitter and the observed wavelength λ_{shift} of the line is

$$v = c\left(\frac{\lambda_o - \lambda_{shift}}{\lambda_o \langle\cos\beta\rangle}\right) \quad (1)$$

where λ_o is the unshifted wavelength and c the speed of light [32]. The observed velocity is only the component parallel to the observation line-of-sight so consideration must be taken of the angle β between the velocity and observation. Therefore $\langle\cos\beta\rangle$ is the line-of-sight average of cosβ weighted by the emissivity profile of the ion. As an example of the degree of accuracy required from the line fitting in the rotation measurements of papers IV, VI and VII, figure 6 illustrates a shift of the order of 0.036nm (3.6 pixels) for the OV 278.1nm line corresponding to a toroidal velocity v_{tor} of 37km/s. For the same example, the fitted experimental width of the line (section 2.3) is 0.13nm (12.6 pixels), with an instrumental width of 0.096nm, corresponding to an ion temperature of 250eV. Results from several reproducible discharges are typically averaged to improve the accuracy of the determined quantity. The apparent small wavelength shift of λ_o in the figure compared to the literature value originates in the wavelength calibration. As both λ_o and λ_{shift} are affected the effect on the obtained velocity is negligible.

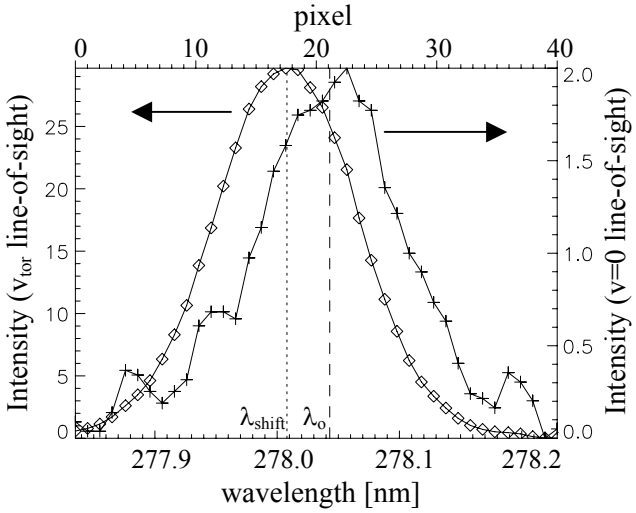

Figure 6: Typical OV line (278nm) as measured on the central poloidal line-of-sight, the zero-velocity position, (right axis and curve with +) and on the mid-plane toroidal line-of-sight (left axis and curve with ◊).

2.3 Line shapes

The shape of an emission line can provide information about the region in which the emitting ion exists in the plasma. For example, the width of a line is influenced by different broadening mechanisms and the magnetic or electric fields can cause splitting.

When strong enough, the local magnetic field affects the shape of emission lines. This is known as the Zeeman effect and is due to a splitting of degenerate energy levels by the magnetic field (interaction of this magnetic field with the magnetic dipole moment associated with orbital angular and/or spin momentum) [7]. A series of closely spaced emission lines are the result, with the spacing determined by the strength of the magnetic field and the relative intensities by the transition rules. The splitting is linearly related to magnetic field strength and can be used to calculate the local magnetic field or locate the position of the emitter if the magnetic field distribution is known [33, 34]. An illustrative case measured in the divertor region of the ASDEX Upgrade tokamak is shown in figure 7. The D_α line is clearly separated into three components. Measurement of the splitting can yield information about the strength of the magnetic field in the emitting region. Analysis of Zeeman line shapes has been made on data from the JET tokamak considering the CIII and BeII features at 465nm and 527nm, respectively. The measurement was made on lines-of-sight through the main plasma that passed through the edge located regions of emission for both ions twice – on the high and low field sides. The question was whether one could in the single measured line shape distinguish the contributions from either side through their different Zeeman splitting, more details of this investigation are in section 4.3 and [35].

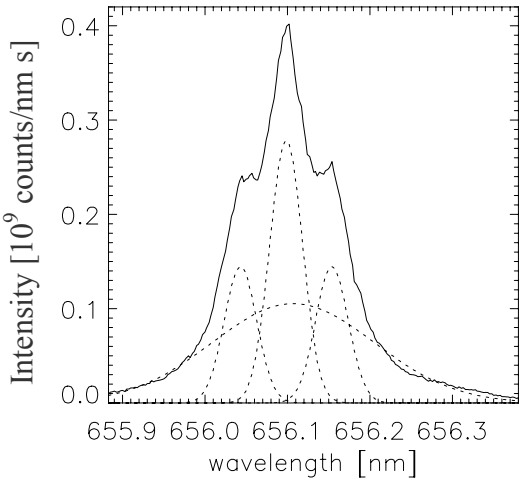

Figure 7: Zeeman split D_α line measured in the ASDEX Upgrade outer divertor (full line) with fitted components (dotted curves) [paper III]. The broad component is included to better match the wings.

Other broadening mechanisms may also play a significant role and the combination of their effects should be included in the analysis [36]. In a relatively low magnetic field device like the RFP, the effect of Zeeman splitting on the line shape is less significant than other sources of broadening and it can be neglected. One such other broadening mechanism is due to the temperature of the emitting ion, which it has gained through collisions with the majority ions in the plasma. This local plasma ion temperature leads to Doppler broadening. The broadening is because the ions have a (Maxwellian) distribution of velocities and as they emit radiation this is both slightly red shifted and blue shifted leading to a broader overall (Gaussian) line shape [37]. The relation between the Doppler broadening and ion temperature T_i is

$$T_i = \left(\frac{c^2\, m}{2\, e\, \ln(2)}\right)\left(\frac{FWHM_{Doppler}}{2\, \lambda_o}\right)^2 \quad [eV] \qquad (2)$$

where λ_o is the unshifted (zero-velocity) position of the line and $FWHM_{Doppler}$ is the full width at half maximum due to the Doppler broadening. Additionally c is the speed of light, e the charge of an electron and m the mass of the ion.

In practice, the broadening due to the temperature must be separated from other broadenings before this relationship can be applied. The Doppler width is separated from the instrumental function width (section 2.1) in the experimental line width (assuming no other broadening mechanisms and using Gaussian line shapes) through

$$FWHM_{Doppler} = \sqrt{FWHM_{Expt}^2 - FWHM_{Inst}^2} \quad (3)$$

Another potential broadening effect is Stark or collisional broadening due to the presence of an electric field. The most important effect is that of the electric field of the nearby particles (electrons or ions), which perturb the energy levels of the emitting ion by changing the potential energy. This causes a Stark shift in the wavelength of the emission proportional to the electric field strength. The initially degenerate components of the line are therefore spread out causing an overall broadening of the line shape [38]. Stark broadening is most significant at high densities. Stark effects in fusion plasmas are the basis of the Motional Stark Effect (MSE) where measurements of the polarisation of the Stark split Balmer emission lines are used to determine the pitch angle of the magnetic fields [39].

2.4 Line intensities

The intensity of emission radiation is also of interest in plasma diagnostics since it is related to the quantity of the ion and to the population of its levels. From the intensity, impurity levels can be determined through atomic (molecular) data and modelling. Most basically, the presence of a particular line or multiplet in the spectrum collected from a plasma indicates that the corresponding ion is present (in the observation region) and is in the required emitting state. For example, the absence of prominent carbon lines in the EXTRAP T2R spectrum indicates that there are no carbon ions in the plasma whilst the presence of chromium in the plasma (resulting from plasma-wall interaction with the stainless steel vessel) is indicated by the occurrence of CrI emission lines. The change in intensity of a line can indicate a change in the plasma conditions, for example influx from the walls or a change in electron temperature bringing higher ionisation stages of an ion into play (as observed in the VUV spectra after the fluctuations described in paper V). More quantitative measurements of the emission intensity are useful for, for example, estimates of the particle fluxes, ion densities or impurity concentrations.

Emission lines can be part of multiplets and it is possible to extrapolate the whole multiplet intensity from a single component. This can be useful where the components are too widely spread to be measured in a single spectral window and as a check on overlying lines that may falsely add to the apparent intensity (for this check, as done in paper I, more than one component is needed so as to provide something to compare with). The extrapolation to multiple intensity I_{IK} from individual line intensity I_{ik} is carried out through

$$I_{IK} = \frac{A_{IK}\, W_I}{A_{ik}\, W_i} I_{ik} \quad (4)$$

with the statistical weights W_i and spontaneous radiative emission probabilities A_{ik} of the individual lines (levels) and of the multiplets (W_I, A_{IK}) [40], where these are obtained from atomic data sources such as [28]. This assumes a statistical population of the multiplet levels. Alternatively I_{IK} is the sum of the individual line intensities I_{ik}.

The first item required for quantitative intensity measurements is absolute calibration (both in terms of intensity and wavelength), this was discussed in section 2.1. Emission modelling often requires a certain equilibrium to be assumed. However, measurements show the plasma emission is not always constant indicating the value of time resolved measurements. In systems where all light in a chosen wavelength window is passed to the detector (for example a monochromator or filter with a PMT detector) calibration means that the fast time development or evolution of the emission and therefore of the plasma and for example the influx of impurities from the walls/limiters can be studied, see paper II results. Systems which measure spectra may not have the same fast time resolution but have the advantage of recording the spectrum (I vs λ) where line shapes, shifts and intensities of multiple lines can be examined. A reliable way to study the intensity of a line quantitatively in such a case is by fitting the spectrum with a single or series of mathematical line shape functions as discussed in section 2.1 (see also paper I) from which the whole intensity (the area and not just the peak or maximum intensity) can be calculated with the appropriate equation.

The intensity or flux of photons in a multiplet Φ_{photon} is related to the flux of the corresponding ion (particle flux $\Gamma_{particle}$) through the relation [40]

$$\Gamma_{particle} = \Phi_{photon} \frac{S}{XB} 4\pi \quad (5)$$

where S/XB is the ionisations per photon with ionisation rate S, excitation rate X and branching ratio B. S/XB is dependent on the electron temperature T_e and density n_e and can be obtained from sources such as ADAS [40]. Particle fluxes are calculated with this method in papers I and II.

Since this relationship can be applied to different lines of the same ion (such as several of the hydrogen Balmer lines) to obtain the same particle flux, the ratio of the intensities of these different lines is equal to the inverse ratio of their S/XB factors. By matching the experimental line ratios, the temperature and density dependence of S/XB can be exploited to estimate T_e and n_e in the emission region. This is done in paper I for EXTRAP T2R.

Ion densities n_i, as in paper VIII or concentrations n_i/n_e as in paper I, can also be calculated from the line intensities through the photo-emissivity coefficient (PEC) for the transition. This is also T_e and n_e dependent.

2.5 Band intensities

We do not only see emission from line radiation in the fusion plasma spectrum. If the conditions are right then it is also possible to observe emission from molecules and molecular ions. Molecular emission is in the form of band structure, as in figure 8. As can be seen in the example, one difficulty with determining the band intensities is that their extent in wavelength means that often atomic lines appear within the band region and additionally the full band may not all be included in the spectral window of the measurement (especially if the resolution is high). A standard solution is to extrapolate to the full band intensity from a reduced unaffected region (with no atomic lines), either the integral in a narrow wavelength range at the band head [41, 42] or from one or more measured vibrational bands (where individual rotational lines are fitted) as in paper III and [43, 44], using molecular modelling. The extrapolation value is generally dependent on factors such as the rotational temperature [45] (since the intensities in the band are determined by it), which must be measured, estimated or assumed.

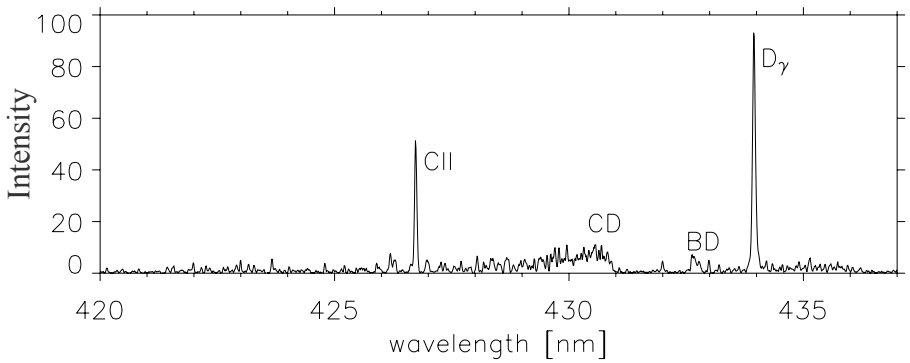

Figure 8: Section of the spectrum measured on the ASDEX Upgrade outer divertor showing the CD (Gerö) and BD molecular bands and the CII (426.7nm) and D_γ lines.

The measurements of the CD Gerö molecular band are, for example, often used in fusion experiments as indicators of the flux of carbon and hydrocarbon impurities and hence the interaction of the plasma with carbon walls (erosion/recycling of C) [42, 45, 46]. Modelling of the band structure and investigations into the changes in the relative intensities of different features in the band were carried out and show that the rotational temperatures and vibrational populations have large effect on whole band appearance and intensity. Figure 9 illustrates the strong rotational temperature dependence of a small section of the CD band. Thus, the appropriate extrapolation factor to apply in order to infer the full band intensity from the measured intensity in a narrow wavelength region changes with different rotational temperature T_{rot}. For instance, the modelling indicates a change in the extrapolation factor (for the 429.5-431nm band head region) from 2.2 to 3.3 with an increase of rotational temperature from 2000K to 5000K – assuming a single rotational temperature for all levels and set vibrational populations (of 1:0.4:0.02 for v=0,1,2) – illustrating the need for caution and further knowledge before blindly applying an extrapolation factor.

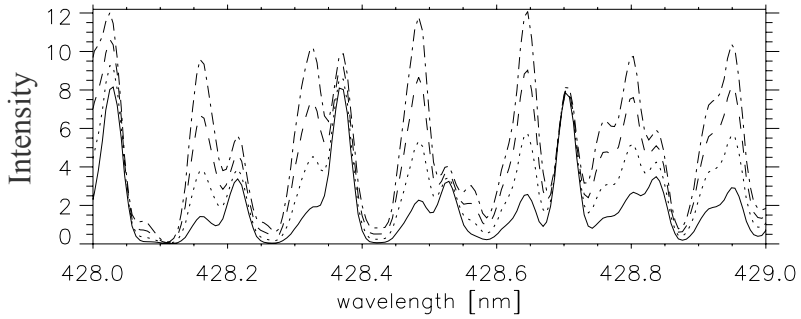

Figure 9: Variation of a section of the modelled CD spectrum with rotational temperature T_{rot} for 2500K (——); 3500K (·····); 4500K (– – –); and 5500K (–·–·–). In each case normalisation is to the 430.68nm CD band feature and one T_{rot} is assumed for all rotational levels.

In the D_2 Fulcher band (d $^3\Pi_u$ – a $^3\Sigma_g^+$) the Hönl-London factors give that the vibrational band intensities can be calculated from the single rotational Q-branch by Σ(P, Q, R-branches) = 2*Q-branch [41]. The whole Fulcher band photon intensity can be extrapolated from the measured vibrational bands using emission cross-sections.

Similar to the atomic case, the molecular particle flux is related to the photon flux (molecular band intensity) although in the molecular case, both ionisations and dissociations per photon must be included [41, 47] and the corresponding D/XB replaces the S/XB factor in equation 5. In some sources D/XB is known as (S+D)/XB. This relationship is exploited in

paper III. If relating, for example, the CD band intensity to the particle flux of higher hydrocarbons such as CD_4 then the dissociation chain must also be considered.

2.6 Molecular temperatures

The intensity I_J of the rotational lines in the molecular band spectrum are related to the upper state rotational temperature T_{rot} [48] through the relation

$$I_J = W_J S_J \nu^3 e^x e^{F_{v'}(J')hc/kT_{rot}(v')} \quad (6)$$

where ν is the frequency of the line, W_J is the statistical weight due to nuclear spin, S_J the Hönl-London factor, and $F_{v'}(J')$ is the energy of the upper state level J' given by

$$F_v = B_v J(J+1) + D_v J^2 (J+1)^2 \quad (7)$$

where all constants (and J) are those of the upper state (and x is a constant determined in the linear fit below). The B_v and D_v are rotational constants and h is the Planck constant, c is the speed of light and k is the Boltzmann constant. Thus, the measured spectrum enables the rotational temperature to be determined through a Boltzmann plot where a straight line is fitted to a plot of the natural logarithm of $(I_J / S_J W_J \nu^3)$ against $F_{v'}(J')$ as in figure 10 – see paper III and [49].

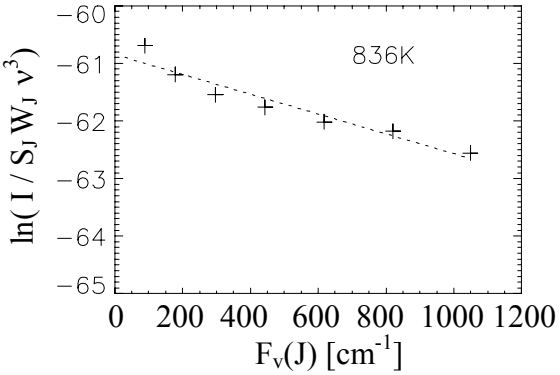

Figure 10: Boltzmann plot for Q-branch lines (Q2-8) of the v=0-0 vibrational band and linear fit revealing a T_{rot} of 836K.

The resulting determined T_{rot} can be used to recalculate the rotational line intensities free from possible disturbance from interfering lines. The relative strength of the vibrational band intensities indicates the relative upper state vibrational populations through the branching ratios and, assuming a thermal population and using Franck-Condon factors from literature, the ground state vibrational temperature T_{vib} can be determined [50].

3. Spatial profiling and lines-of-sight

One issue inherent to spectroscopic diagnostics is that the instrument measures light collected along a line-of-sight through the medium of interest, which generally means that the photons do not originate from one localised position. There are exceptions where, for example, the source of light is due to interaction of the plasma constituents with a neutral beam that crosses the diagnostic line-of-sight (as in figure 11) resulting in the source (the interaction region) being at a particular location in the line-of-sight (the crossing point with the neutral beam). For instance, this principle is exploited in charge exchange with neutral beam injection (NBI) and the MSE spectroscopy mentioned in section 2.3. Similarly, injection of particles into the plasma (gas puffing) can give a localised source of emission. In other cases, the light can be emitted over a substantial fraction of the line-of-sight.

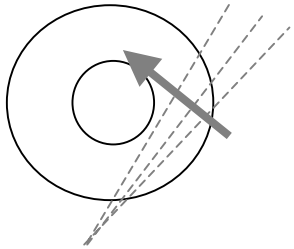

Figure 11: An array of lines-of-sight intersecting a neutral beam (thick arrow) can be used for spatial profiling through localised emission where the plasma interacts with the beam.

It can be useful to have an idea of from where an emission occurs, for example to choose the right line-of-sight for a particular observation. If an ion is located in the core of the plasma then the emission will also be from the centre of the plasma and to measure this emission a line-of-sight that will pass through the region of emission and not just the edge is needed.

For some spectroscopic measurements the spatial dependence of a parameter is of primary interest. Methods for radial or spatial profiling vary. However, most rely on the principle of collecting information from several spatial points simultaneously. Frequently, multiple or crossed lines-of-sight are used. Alternatively, multiple emitting ions located at different positions can be used or a localised emission source (as described above) [51]. Injection of particles, through a beam or gas puffing, will affect the plasma and in such a case the spectroscopy can no longer be considered to be a passive diagnostic.

It will be shown here that spatial profiles play an important role in spectroscopic measurements of fusion plasmas. They can affect what is observed, can be the aim of the measurements and can give vital information about the local plasma conditions. Radial or spatial profiling is a useful tool in the arsenal of spectroscopy.

3.1 Where the line-of-sight choice is less important (central line-of-sight)

In some aspects or applications of spectroscopic fusion diagnostics the choice of line-of-sight is less important or a simple line-of-sight that passes through all regions of the plasma (including both the edge and core) is appropriate. For instance, in the survey scan of the EXTRAP T2R plasma to identify the impurities in paper I a central poloidal line-of-sight passing through the r=0 position (therefore traversing the whole plasma as in figure 12) was used. The different ions seen in the spectrum can be emitting from different regions of the plasma. However, the different emission locations were not treated as important as it was not central to the application at hand. The observed spectrum may have had some differences if an alternative offset line-of-sight had been used because emission lines from very central ions may not have been present. Relative intensities would also have been different, however, again this was not important for the line identification.

The same line-of-sight is also used in other parts of this research and implicit in the use of this 'central' line-of-sight is the assumption that the plasma is centred on r=0. Additionally, for some applications it is assumed that the plasma is cylindrically symmetric about r=0, see also the discussion of the radial profiling in section 3.4. With the broad emission profiles in EXTRAP T2R small excursions of the plasma from its central position will not make significant changes to the observed spectra.

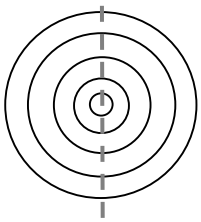

Figure 12: Central poloidal line-of-sight through the r=0 position. Concentric circles are drawn for emphasis.

3.2 Line-of-sight viewing cone

The central poloidal line-of-sight is also used to determine the zero-shift wavelength of the emission lines for the EXTRAP T2R plasma rotation measurements because it is perpendicular to both the poloidal and toroidal components of the rotation (figure 13). In addition to assuming the plasma is centred cylindrically on r=0, we assume that the spread of the line-of-sight cone is not significant (essentially that it is a narrow cylinder) in that at the opposite side of the plasma from the fibre we can still consider the motion and viewing angle to be perpendicular to each other.

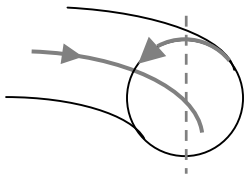

Figure 13: The central poloidal line-of-sight (dotted line) is at right-angles to both the poloidal and toroidal components of the rotation (arrows).

The spread in the line-of-sight viewing cone (figure 14) is determined by the collection optics on the transmission fibre (or possibly by the geometry of the recessed port if the spread is large). For the EXTRAP T2R velocity measurements, experiments with the fibre in question point towards a small angle (~1.3^o) of spread (symmetric in 2-dimensions). This means that the viewing cone does not touch (by a large margin) the edges of the recessed port opening at the vessel wall so this does not restrict the cone. Furthermore, at the opposite side of the vessel the whole of the viewing cone enters the facing recessed port and impinges on the port (for example 50mm diameter) with a spot size of ~11mm in diameter. At the start of this section it was stated that this line-of-sight was used to measure the zero-velocity position of the spectral lines because it was at right-angles to the toroidal and poloidal rotation. Calculations show this is still a reasonable approximation at the extreme edges of the viewing cone on the far side of the vessel where the β angle in equation 1 in section 2.2 is close to 90^o (~89^o).

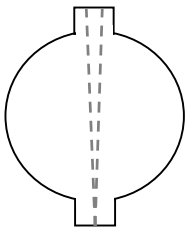

Figure 14: The line-of-sight is not a one-dimensional line but instead consists of a cone that spreads out. The angle shown here is exaggerated compared to that of the fibre used for the EXTRAP T2R rotation measurements.

The tangential mid-plane toroidal line-of-sight used for the toroidal velocity, labelled 81^o in figure 3, is significantly longer than the poloidal line-of-sight considered above, which means that by the far side the viewing cone has spread out more and will not all enter the recessed port. The wall is at an angle to the line-of-sight normal so the projection of the spot will be larger than if the wall was at right-angles to the line-of-sight. A spot of ~7cm diameter is obtained. The effect of the spread is not included in the velocity calculations but only results in a very small change in the angle β at the plasma edge. In these viewing cone calculations it was assumed that the cone angle was not affected by passing through the entrance window.

In the ASDEX Upgrade divertor experiments differences were seen between the measurements on the wide-angle (spot size on wall ~7cm) and narrow (spot size ~1cm) lines-of-sight, for example in the fraction of the gas puff observed.

3.3 Electron temperature and density profiles

We mention in passing the assumptions on the electron density (n_e) and temperature (T_e) profiles. T_e and n_e come into play when dependent atomic (or molecular) parameters, for instance the S/XB or photo-emissivity coefficient (PEC), are included. In EXTRAP T2R we have generally had measurements of the line-averaged n_e from a two-colour interferometer and on-axis T_e from Thomson measurements, at a single time point. Earlier studies [52] of the radial profile of n_e showed a parabolic profile of the form

$$n_e(r) = n_e(a) + \left(n_e(0) - n_e(a)\right)\left(1 - \left(\frac{r}{a}\right)^{\alpha}\right)^{\gamma} \qquad (8)$$

where a is the minor radius and α and γ are profile parameters, for example α=2 and γ=1 in paper VIII. Where necessary recent assumptions as to the profiles have been based on this form (for T_e also) with the limiting n_e from measurements where possible. The consistency of our assumed profiles are checked relative to the measurements that are available (for example VUV, bolometer radiated profile or interferometer measurements [53]). In the ASDEX Upgrade divertor, there are complementary Langmuir probe measurements at the wall.

3.4 Radial profile of emissivity : an example

The radial profile of the emissivity of an emitting ion is important for a variety of applications including the determination of ion densities (profile or concentration) and in the calculation of the angle correction factor between line-of-sight and rotation for ion velocity calculations. As discussed above, there are a number of ways in which the line intensity can be obtained at multiple radial positions. There are also various different techniques to establish the radial profile from these spectroscopic measurements [54].

A standard approach is through Abel inversion where measurements on a number of lines-of-sight can be mathematically inverted to obtain the radial profile [55]. The method relies on the quantity under measurement (such as emissivity or refractive index) being cylindrically symmetric. Additionally, the success of the inversion is limited by the number of line-of-sight integrals that can be measured. A restricted set of radial points (lines-of-sight) will only give limited radial information; interpolation is needed introducing further assumptions.

An alternative approach is to fit a modelled emission function with free parameters to the observed data points. This is the procedure used in paper VIII in EXTRAP T2R and as an illustrative example of the technique and the assumptions we will discuss it here. A set of five lines-of-sight in one poloidal section (see figure 15) is used where the output from all of the fibres meet the spectrometer slit in a vertical array (the radiation on all lines-of-sight is simultaneously measured at the same wavelength) and detected by individual PMT detectors. The impact factor of each line-of-sight allows the measured intensities from the chosen emission line to be plotted against minor radius. An asymmetrical Gaussian model of the form

$$\varepsilon(r) = c_1 \exp\left(- \left(\left((r/a) + x \right) \frac{(r/a) - c_2}{c_3} \right)^2 \right) \left(1 - (r/a)^4 \right) \qquad (9)$$

is assumed for the modelled radial profile of ion emissivity, where a is the minor radius and c_1 to c_3 are the free parameters. The method relies on choosing the right emission profile shape (or a reasonable approximation of it) to fit within the free parameters. The chosen shape is based on the experimental data with asymmetry added to avoid divergence of the ion density profiles given the rapid n_e decline at the edge.

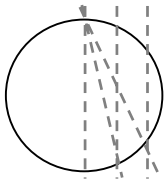

Figure 15: The array of five lines-of-sight used for the determination of the radial profile of the ion emissivity [paper VIII].

The radial profiles of the emissivity of the oxygen ionisation stages OII to OVI, and the neutral ions MoI, CrI and FeI were reconstructed, as shown in figure 16. Broad and

overlapping profiles for the higher oxygen ionisation stages (with emission over a large fraction of the radius) were obtained. The lower ionisation stages were narrower and peaked closer to the edge and the neutral metal profiles were even more towards the edge. An alternative novel method of determining the normalised emissivity profiles through analysis of the correlation of fluctuations in the emission on the different lines-of-sight gives similar profiles in paper IX.

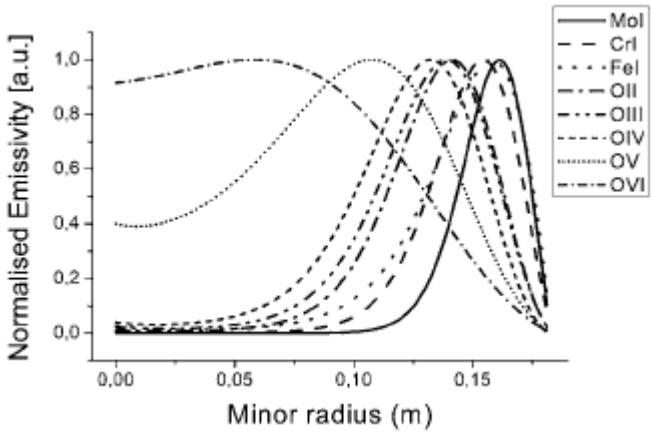

Figure 16: Calculated normalised radial emissivity profiles for the OII to OVI and CrI, MoI and FeI ions from paper VIII.

In calculating the profiles assumptions are made that we have cylindrical symmetry (of the plasma and of the emissivity profiles), that the plasma is centred on r=0 and that the impact factors of the lines-of-sight are well defined (both the direction and spread of the viewing cone). Small correction factors were also required to account for different reflections and losses in the lines-of-sight.

Once the emissivity radial profiles were obtained, radial profiles of the ion densities were also determined (through the use of atomic data in the form of photo-emissivity coefficients).

3.5 Toroidal rotation profile

In this section the radial profile of the toroidal rotation on EXTRAP T2R will be discussed. Rotation profiles have also been studied through Doppler shifts of intrinsic impurities at other machines including the RFX [32] and MST [56] RFPs and the TdeV tokamak [57]. In other experiments charge exchange recombination spectroscopy is utilised for rotation profile studies [58, 59]. In interpreting the results we have assumed that the local ion temperature and velocity measurements from the impurity ions can be applied to the main plasma.

The radial emission profiles for the different oxygen ions in EXTRAP T2R from paper VIII are used to calculate the correction factors to the plasma rotation velocities (calculated from the Doppler shift) due to the angle β between the line-of-sight and the flow (see figure 17 and equation 1). The variation in $\langle\cos\beta\rangle$ – the line-of-sight average weighted by the respective measured $\varepsilon_i(r)$ – for the oxygen ions is not large with, for example, $\langle\cos\beta\rangle$ of OII being 0.909 whilst that of OVI is 0.966. Therefore, unless the profiles are radically different then only a small error can be introduced in the $\langle\cos\beta\rangle$ factor for the velocity determination.

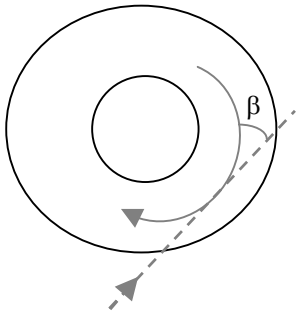

Figure 17: The angle β between the toroidal rotation (curved arrow) and the mid-plane toroidal line-of-sight (dashed arrow).

In paper IV the toroidal rotation velocities of the OII to OVI ions were measured in EXTRAP T2R using the Doppler shifts of spectral lines as described in equation (1) and section 2.2. For OII to OVI the spectral lines at 441.5nm, 376.0nm, 338.6nm, 278.1nm and 343.4nm, respectively, were used. Together with the measured normalised ε(r) and the line-of-sight geometry, the radial profile of the toroidal velocity was reconstructed. A radial profile of the toroidal velocity v(r) was assumed (a parabolic profile was found to be best) and, along with the emissivity profiles $\varepsilon_i(r)$ of OII to OVI and the variation in cosβ with radius, was converted to a line-of-sight profile – figure 18 shows the $\varepsilon_i(l)$. The line-of-sight integral of the product of v(l) and cosβ(l), weighted by $\varepsilon_i(l)$, gives a single value of the velocity for each ion. This is compared to the experimental values calculated by equation 1 and v(r) is improved iteratively. Figure 19 shows the resulting v(r) obtained.

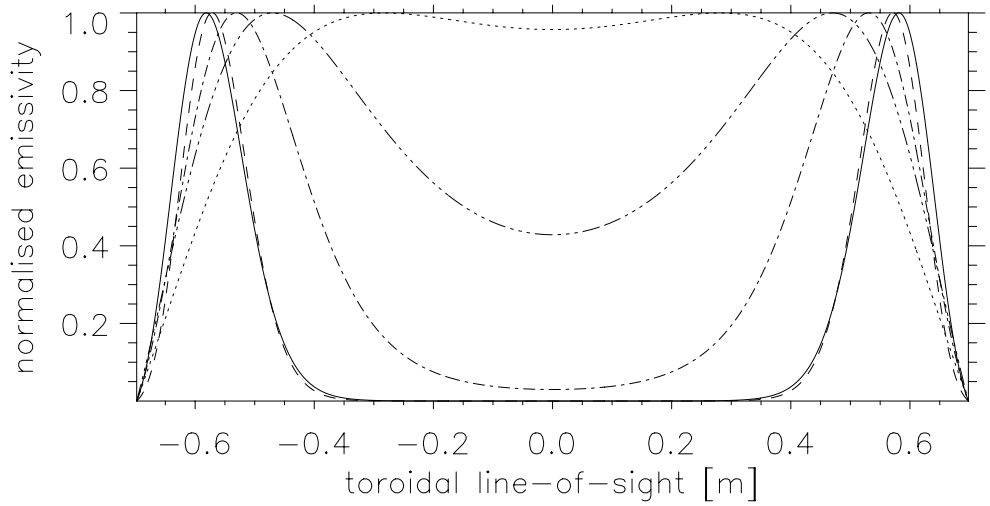

Figure 18: Normalised emissivity profiles along the mid-plane toroidal line-of-sight for the ions OII (——), OIII (– – –), OIV (– · –), OV (– ··· –) and OVI (·····). Converted from radial profiles measured with the five-channel spectrometer described in papers VIII and XI.

Any uncertainty in the emissivity profiles of the ions, in particularly in the assumption of poloidal symmetry, is carried through to the resulting v(r). For this discharge series the emissivity profile does not change significantly and the reconstruction is done for a single time point. The velocities obtained and used for the reconstruction are an average over several reproducible discharges. Additionally, we have the assumptions of negligible spread in the line-of-sight viewing cone and exact set direction of the line-of-sight. The assumed shape of v(r) is obviously significant. However, various profiles were investigated as part of the work, including a slope, a step and a sloping step, and the resulting modelled ion velocities did not have the correct relative magnitudes. A more complex profile is ill advised

due to the limited number of radial points (ions). A fair agreement is seen in the experiment with the exception of the OII, which is experimentally too dissimilar to the OIII. The experimental emissivity radial profiles of the oxygen ions used here and in the investigation of the profile of the ion temperature T_i in section 3.6 do not include the (small) core asymmetry term in equation (9).

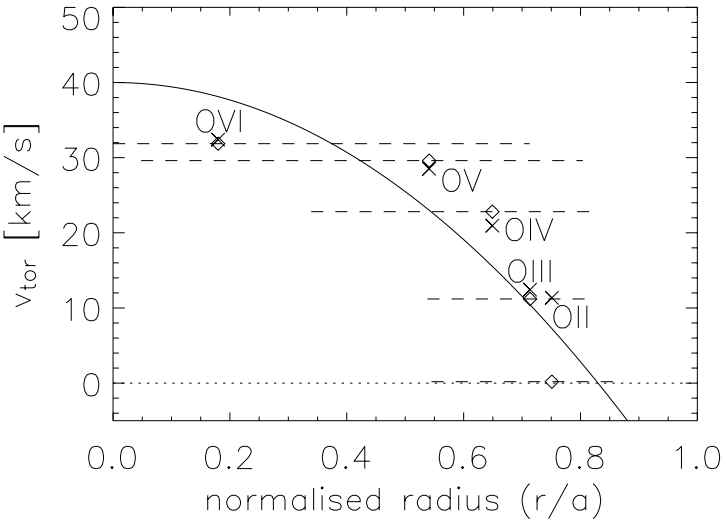

Figure 19: Reconstruction from paper IV of the radial profile of the toroidal ion velocity $v_{tor}(r)$ (solid line), which results in the modelled (x) ion velocities v_i. The experimental velocities (◊) at a single point are shown for comparison. The horizontal dashed lines indicate the FWHM of the emission curves whilst the points are plotted at the radii of their respective emissivity peaks.

3.6 Radial profile of ion temperature $T_i(r)$

As described in section 2.3, the ion temperature can be derived from the Doppler broadening. Measurements of the evolution and the radial profile of the ion temperature in EXTRAP T2R shall be discussed in this section. Ion temperature studies on RFPs have also been made in, for example, MST [60] and at RFX [61] using Doppler broadening. On EXTRAP T2 ion temperature measurements [62] revealed an anisotropy in the ion temperature between the toroidal and poloidal directions ascribed to heating primarily parallel to the magnetic field. This is in contrast to measurements on MST [60] where such a difference in the ion temperatures is not observed.

The evolution of the impurity oxygen ion temperatures was studied with the same spectroscopic measurements taken for the ion toroidal rotation study in paper IV and discussed above in section 3.5. An example of the line shape and width to temperature correspondence was given in figure 6 and section 2.2. Similarly to the ion velocities, the results are averages over several discharges. As the figure 20 shows, the temperatures are fairly constant throughout the discharge and do not show much difference with the application of the partial coverage mode stabilisation feedback system in operation at that time (more details in paper IV and in section 4.1). The error bars indicated are the average uncertainties for each ion, calculated from the uncertainty in the line fitting. The higher ionisation stages have a hotter temperature than the lower stages nearer the edge as demonstrated by figure 21. More recent measurements of the ion temperature of OV with the full feedback system in paper VI show T_i rising slowly (and maintained at a higher value) throughout the extended discharge.

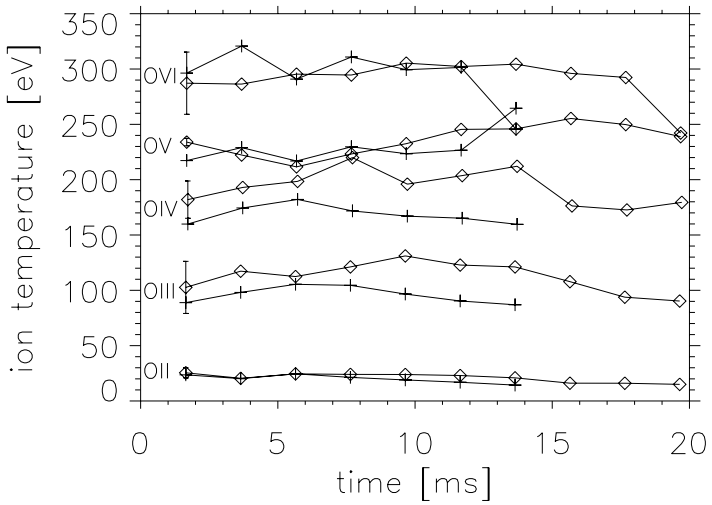

Figure 20: Time evolution of the measured the OII to OVI ion temperatures for the discharge cases with feedback mode stabilisation (◊) and without (+). The average error bars for each ion are indicated on the first point of each curve with feedback.

Following a similar procedure to the reconstruction of the toroidal rotation radial profile (see paper IV and section 3.5), the radial profile of the ion temperature T_i was investigated. A simple form for $T_i(r)$ is first assumed. For each ion a Gaussian shape for the line radiation is taken at each point along the toroidal line-of-sight (horizontal in the mid-plane tangential to the r=0 position). The intensity of each curve is set by the height of the normalised emissivity profile for the ion at the corresponding location. The 'experimental' width of the curve is determined, through equation 3 in section 2.3, by the instrumental width of the spectrometer at the ion's wavelength and the Doppler width due to the ion temperature at the corresponding point on the line-of-sight. The wavelength position of the curve is determined by the Doppler shift due to the parabolic toroidal velocity profile determined in paper IV (taking into account the angle between the line-of-sight and rotation as only the velocity component in the direction of the line-of-sight causes the wavelength shift). A sum is taken along the line-of-sight of the Gaussian curve at each point to give the total (theoretical) spectral curve.

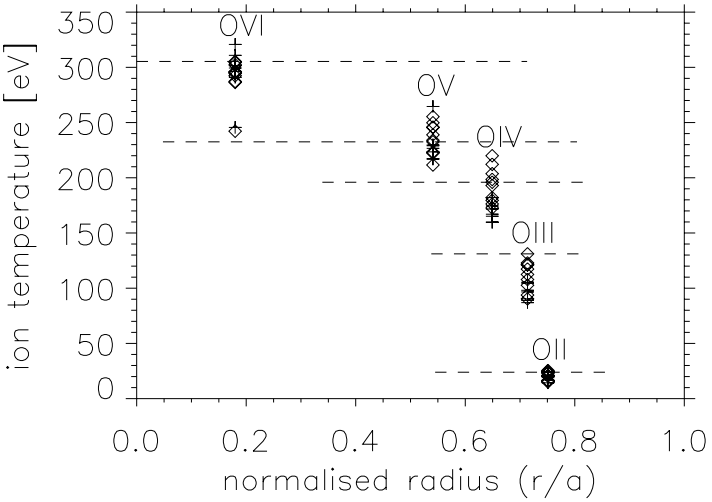

Figure 21: The measured T_i of figure 20 as a function of radial position of the ions. The points (◊ with feedback and + without) are plotted at the radial position of the peak in the respective ion emissivity profiles and the horizontal dashed lines represent the FWHM of these curves.

For reasonable forms of the radial profiles (temperature and velocity) the summed curve is fairly symmetric. This would seem to indicate that measuring the temperature on the toroidal line-of-sight does not add additional broadening to the spectral line than if measured on a line-of-sight without influence of the rotation (such as the central poloidal line-of-sight).

A single Gaussian is then fitted to this summed curve and the Doppler width deconvolved from the fitted width and equation 2 used to obtain the ion temperature. By comparing the derived T_i to those experimentally measured (selecting a typical single time point) for each of the OII to OVI ions the assumed $T_i(r)$ can be improved. The rapid fall off in temperature for the lower ionisation stages observed experimentally is hard to reproduce with a simple parabolic profile $T_i(r) = T_i(r = 0)*[1-(r/a)^2]$. The measured emissivity curves for OII and OIII from paper VIII are very similar, which is the reason that it is difficult to match the disparity in their experimental T_i with the results of the $T_i(r)$ modelling. The separation between T_{OVI} and T_{OV} is also reduced in the model results and if one aims for a match of T_{OVI} then the other T_i are larger than the experiment as can be seen in figure 22(a). In contrast, if one aims for a match of T_{OV} and T_{OIV} then T_{OVI} is too small – although T_{OIII} is reasonable – as shown in figure 22(b).

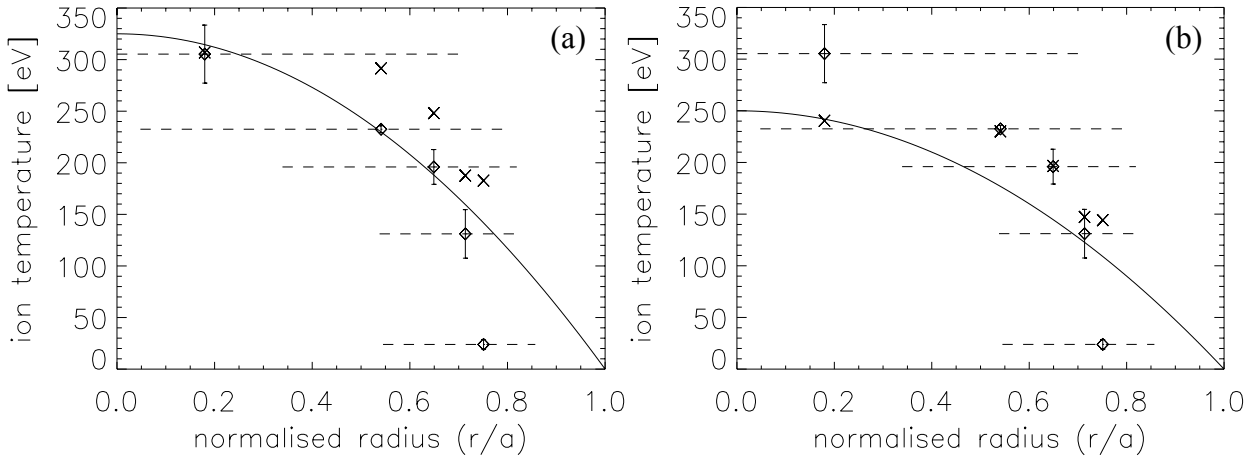

Figure 22: The modelled parabolic profile (full line) assumes (a) $T_i(r=0)=325eV$ and (b) $T_i(r=0)=250eV$. The corresponding T_i calculated for each ion is given by (×) and is to be compared with the experimental T_i (◊), taking the data from the feedback case at 9.6ms. The points are plotted at the peak of the respective emissivity profiles (OII to OVI sequentially from the edge inwards) and the dashed lines represent the FWHM of the emissivity profiles.

The emissivity profiles of the neutral metallic ions (Mo, Cr and Fe) were measured to be slightly closer to the edge so they could potentially give an additional radial point to help establishing the T_i profile. Some measurements in CrI and MoI were made at the same time as those for the oxygen ions. However, there are issues with the experimental width being so close in size to the instrumental width. This means that sometimes the fitted experimental width appears to be fractionally less than the instrumental width, which causes problems. Low temperatures of the order of that determined for OII are obtained where widths are suitable although with large errors (such as 20±20eV).

3.7 Spatial profiling (in the tokamak divertor)

Profiling or profile reconstruction need not only be in terms of radius. In particular, there are some geometries, for example in a tokamak divertor, where we might be more interested in a different spatial reference plane. Rather than relate to a fixed spatial position it may also be fruitful to relate a quantity to a particular aspect of the plasma that may move during the discharge, for example the strike point of the last closed flux surface (LCFS) on a divertor target.

An example of this is taken up in the study of the D_α radiation in the ASDEX Upgrade divertor plasma in paper III. Looking in the outer divertor (as in figure 23) we assume the intensity of the D_α radiation to be related to the proximity of the strike point of the LCFS on the divertor wall and use measurements on an array of lines-of-sight (narrow ~1cm spot size) during a sweep of the strike point to plot the intensity as a function of strike point proximity rather than time as shown in the dotted curves of figure 24. Although the small discrepancies in the overlapping regions of the different lines-of-sight indicate our assumption (that intensity was proportional only to the proximity) to not be completely true, we are able to reconstruct a profile of the emission (the solid line in figure 24) by taking the average intensity in small space intervals. Comparing this profile to that measured with a second spectrometer on interlaced lines-of-sight on the same array a relative calibration of the two spectrometers was accomplished (at the D_α wavelength), enabling absolute intensity calibrated measurements to be made when only one spectrometer was independently calibrated. The profile also demonstrates the increased emission when the strike point was closest to the point of observation. When similar molecular D_2 measurements were added the spatial distribution along the divertor wall of the molecular contribution to the D_α radiation could be calculated.

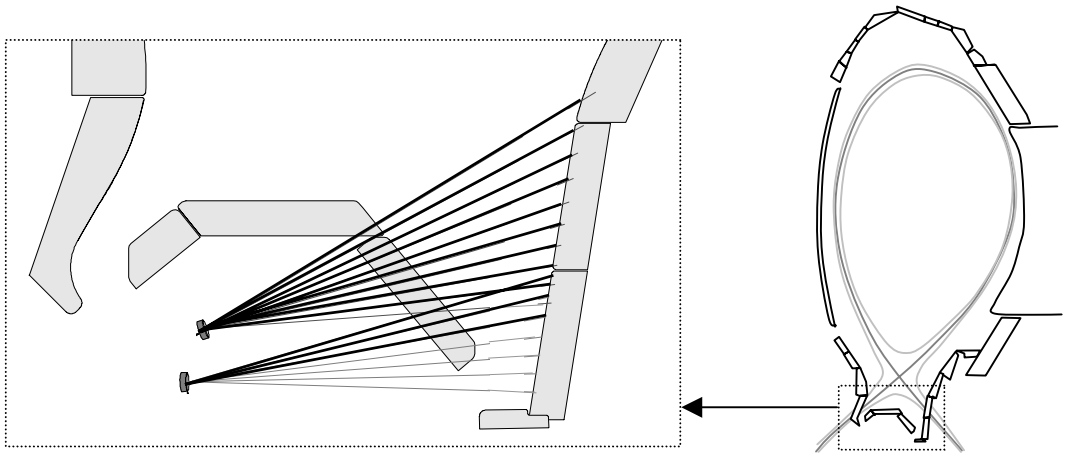

Figure 23: Cross-section of ASDEX Upgrade with enlargement of the divertor region showing the outer divertor line-of-sight array, the darker lines-of-sight were those used in the experiments of paper III.

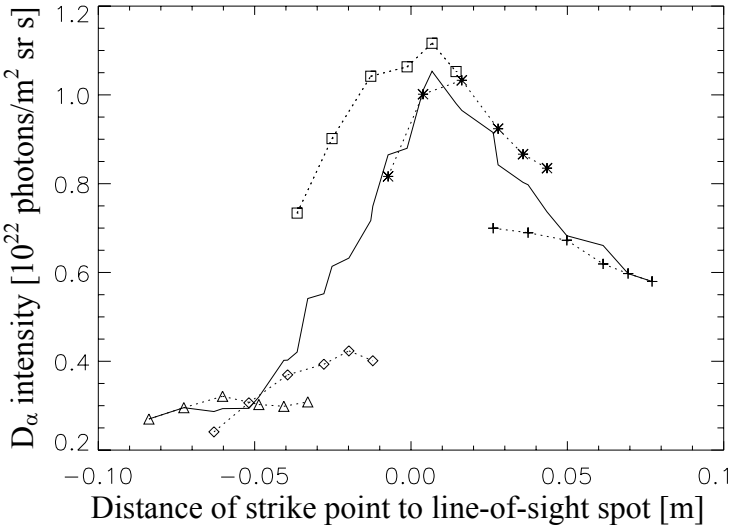

Figure 24: The D_α line intensity measured during the strike point sweep where each symbol type corresponds to measurements on a different line-of-sight in the array. The solid line represents the reconstructed profile of the intensity [paper III].

It should be stressed that whilst in general the spectral line intensity is determined by the radial profile of the emissivity and by the atomic processes in the plasma as a whole and so is dependent on the radial profiles of T_e and n_e (T_i only comes in when charge exchange processes are important in the production of the emission), in this section the neutral ion intensity has been examined. For neutrals (and single ionised ions), most of the intensity is related to atomic processes at the edge, in other words to plasma wall interaction and particle flux. The profiles of T_e and n_e are not important for the intensity of D_α since the emission comes from the edge.

4. Applications of spectroscopy

The strength of spectroscopic measurements in fusion plasmas is not just that it is possible to measure such quantities as the plasma rotation, ion temperature or particle influx as has been discussed above, but rather what these measurements can tell us about the plasma and the discharge scenarios that are operating. In this chapter I will discuss some of the areas in which visible spectroscopy has been applied in this thesis, focussing on what and how the spectroscopic diagnostics add to the broader picture of the plasma and the operating conditions.

4.1 Control and confinement

A major issue in the development of fusion is the control and confinement of the plasma and the majority of the work in this thesis can be related to information diagnosis in these areas. It is constructive therefore to say a few words about the control schemes and confinement issues and what the spectroscopy can tell us in this context.

Unstable resistive wall modes (RWMs) are a feature of thin shell RFP devices without a perfectly conducting wall. The inability of a passive wall to act as such introduces the need for active control of these MHD (magnetohydrodynamics) instabilities [61]. Control of RWMs is also important for tokamak advanced scenarios and future reactors. Stabilisation has been shown to be possible through sustained plasma rotation and through feedback stabilisation of the modes or through a combination of the two, as described in paper VI and [61, 63, 64].

In the case of stabilisation by sustained plasma rotation, the resistive wall can be made to appear to be perfectly conducting if it is rotated relative to the plasma (or vice versa), avoiding locking of the plasma to the wall. A non-uniform rotation is more efficient. Stabilisation is principally due to the destruction of the coherence of the mode structure and calculations show that a modest amount of shear flow, from for instance NBI, would be sufficient to stabilise the RWM without additional feedback [63] where the calculations are for the large tokamak experiments DIII-D and ITER.

Active feedback mode control or stabilisation has many variants. However, essentially loop sensors are used to read the radial field at or near the torus surface and currents calculated by an algorithm are applied to control coils to locally cancel the field thus mimicking an ideal conducting wall. Different schemes act on single, multiple or the full mode spectrum and various controller systems have been used. Active feedback control experiments are central to the EXTRAP T2R scientific program.

In EXTRAP T2R without feedback control the multiple RWMs grow causing an increasing amplitude of the radial field component at the wall and the initially rotating tearing

modes (TMs) are slowed by non-linear torques. Below a certain rotation, the modes lock to the wall and rapid growth of the radial field is seen. Plasma wall interaction occurs leading to increased plasma resistivity and an increase in the toroidal loop voltage. With active feedback control (of which various forms have been successful) the growth of all m=1 modes is suppressed and the rotation of the TMs is sustained. The loop voltage is maintained and axi-symmetry of the LCFS is improved lowering plasma wall interaction and avoiding the large influx of impurities.

The dramatic change in the interaction of the plasma with the wall and hence the impurity influx is clearly demonstrated by the spectroscopic time traces of the line radiation from the neutral ions of MoI and CrI, representing interaction with the limiter and wall respectively as seen in figure 25, and in papers II, VI and VIII. Additionally, the small increase in hydrogen influx at the discharge end is reduced. The difference in the plasma wall interaction between the discharges with and without active feedback mode control is also investigated in the discharge-averaged measurements made to calculate the calibrated particle influx in paper II and section 4.4. In that paper the molybdenum and chromium spectroscopic results are in good agreement with collector probe measurements.

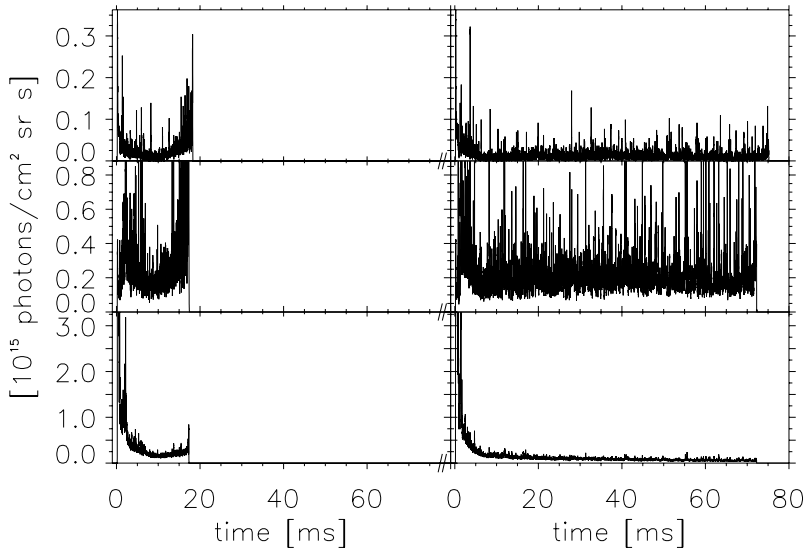

Figure 26: Typical evolution of the intensities of neutral impurities in a standard discharge (left) and in a discharge with active feedback stabilisation of the modes applied (right). The top panels show MoI (line at 319nm), the centre panels show CrI (multiplet at 359nm) and the lower panels show H_α.

The results obtained from visible spectroscopy, that is to say the increased radiation losses in the latter half of the non-feedback discharge and its suppression in the feedback case, are also observed in other spectroscopic diagnostics such as the VUV and SXR radiative power losses and total radiative power loss (the sum of VUV and SXR) from bolometers.

As detailed previously, the plasma rotation has been determined in papers IV, VI and VII from the measured Doppler shift of emission lines of the impurity ions. Thus, the spectroscopy allows us to see how the plasma rotation is affected by the use of feedback control schemes and how it relates to other quantities, for example mode rotation. It is demonstrated that the use of feedback causes a slightly increased toroidal plasma rotation in the initial acceleration phase and causes the high velocity to last for a longer period. The rotation was in the same direction as the plasma current. There was good agreement with the tearing mode rotation (comparing an ion and m=1 mode at similar (central) location) with the two having a similar magnitude velocity in the same direction and a similar time evolution.

This was also the case for the poloidal rotation, within uncertainties and mode profile assumptions. It is speculated that the increased plasma rotation in the initial phase with feedback may help sustain the tearing mode rotation compared to the non-feedback case. The earlier wise shell feedback stabilisation experiments (paper IV) with the active coils covering only 50% of the plasma surface showed a slow down in the plasma and mode rotation at later times (coincident with the increase in radial field associated with the mode). However, the later intelligent shell feedback experiments with 100% coverage (paper VI) had a constant or slightly increasing plasma rotation (with the non-feedback case here also having less slow down). The difference is illustrated in figure 26 for the OV ion.

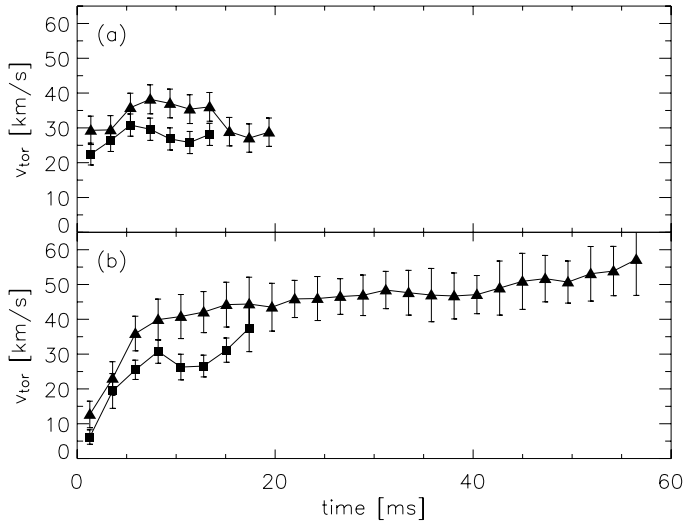

Figure 26: Evolution of the OV toroidal rotation velocity for discharges with (▲) and without (■) active feedback stabilisation in the cases (a) paper IV and (b) paper VI.

Spectroscopy also gives the ion temperature from the Doppler broadening, which is studied for the OV (a central ion) in the active feedback mode control context in paper VI. Like the rotation, the temperature (assumed to be representative of that of the protons) initially increases during one wall time (~6ms). In the standard case the temperature then remains constant whilst in the (full) feedback case the temperature continues to rise slightly though at a slower rate. A similar initial rise is seen in the on axis electron temperature (measured by Thomson scattering) although the absolute level is less than that of the ion (and no change is clear with respect to feedback usage).

The spectroscopic diagnostics are beneficial as they add to the information that can be gleaned from the experiments and aid the understanding and interpretation of the degree of success of applied plasma control schemes.

4.2 Improved confinement – PPCD

Pulsed poloidal current drive (PPCD) is an operating scheme where current is driven at the edge to change the current profile and improve particle confinement. It has been studied at various devices [56, 65, 66]. In papers VII and VIII it is investigated in EXTRAP T2R. In EXTRAP T2R single PPCDs (of ~3ms) are generated by inductively applying poloidal electric field at the edge (of 1.5-3Vm^{-1}) during the current flat-top. The primary indicator of PPCD performance is taken to be the SXR detector where a significant increase in signal is observed indicating an increased electron temperature [56]. Other effects are a change in the

equilibrium – a deeper reversal (F more negative) and higher pinch parameter θ – and a decrease in resistive loop voltage (so a higher T_e, also seen in the Thomson measurements) with all parameters returning to pre-PPCD levels after the PPCD.

Spectroscopic measurements of visible wavelength line radiation of the neutral ions chromium, iron, molybdenum and hydrogen with monochromators and H_α filters show a reduction in the emission activity during PPCD. The usual (non PPCD) emission time traces, which indicate the impurity influx from the wall and limiters, are characterised by fluctuations and intermittent bursts. During the PPCD there are fewer and smaller peaks, which may indicate reduced plasma wall interaction and improved particle confinement through suppression of the magnetic reconnections (by current profile changes) and of the electrostatic turbulence (by deeper reversal and increased magnetic shear). Changes in the effect on the spectroscopy traces were observed with different amplitudes of the applied PPCD indicating performance changes.

The measurement of the (centrally located) OV ion toroidal velocities by Doppler shift do not show an increase with the PPCD, a result which is also seen in the tearing mode helical angular phase velocities studied. During PPCD the electrons are heated and this energy is given to the ions as is seen in the increased OV ion temperature from the Doppler broadening after the PPCD.

Emission profiles of the oxygen ions OIV and OV and the implications for particle transport (diffusion) are also studied during PPCD in paper VIII and show that in the core profile changes are due to reduced particle transport whilst at the edge there is less effect on the particle transport and T_e changes can explain the differences seen.

Thus, the spectroscopy diagnostics add to the information gathered during the PPCD experiments and can add to the understanding of the effects.

Improved performance for RFPs is also indicated when the plasma enters a quasi-single helicity (QSH) regime [63]. Here a single tearing mode spontaneously grows to become dominant over the decreased secondary modes leading to improved performance. Investigation of this regime in conjunction with the EXTRAP T2R mode control feedback system is ongoing [68].

4.3 Location of emitting ions through Zeeman analysis

Spectroscopic measurements can, as discussed in section 2.3, tell us about the magnetic field strength through the Zeeman splitting of the line radiation. Turning the problem upside-down, knowing the field strength (through some other measurement technique) spectroscopic measurements of the line shape can tell us about the location and density of the emitting ions in the plasma (the local plasma environment) [34].

As an illustration we can consider analyses carried out at the JET tokamak as part of the research included in this thesis. A line-of-sight through the main plasma transverses the outer regions twice (figure 27) and hence the measured line radiation of an ion that is located towards the edge will have contributions from both outer regions. In a tokamak environment such a horizontal line-of-sight will therefore have contributions from both the high and low field sides where the local plasma surroundings may be different.

The erosion and redeposition of beryllium (Be) changes the quantities of Be and carbon (C) ions in the plasma edge region following the addition of a coating of Be on the carbon plasma facing wall components at one side (with the aim of reducing the influx of carbon into the plasma) [35].

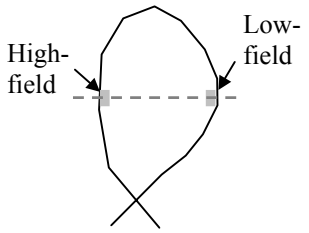

Figure 27: Sketch of the cross-section of the JET plasma showing the line-of-sight passing through the two edge emission regions, at the low and high magnetic field sides.

The known high and low-field magnetic field strengths in the approximate region of emission (this is assumed to be at the edge) are used to model the Zeeman splitting for the emission feature. A Doppler broadening (from the local temperature measurements) is added to the instrumental width for each Zeeman component and the resultant total line shape calculated. The relative strength of the contributions from the two sides of the tokamak is determined by fitting a sum of the line shapes in the two regions to the experimentally measured line shape.

Line radiation of the BeII (527nm) and CIII (465nm) features was monitored and, although the relatively low magnetic field gradient made it harder to distinguish the components, preliminary analysis indicated a very slightly stronger contribution of CIII from the low-field side rather than the high-field side and fairly equal BeII contribution strengths for the example shown in figure 28. Thus, analysis of the measured spectral line or feature shapes can provide us with information on the plasma environment and success of impurity influx reducing measures.

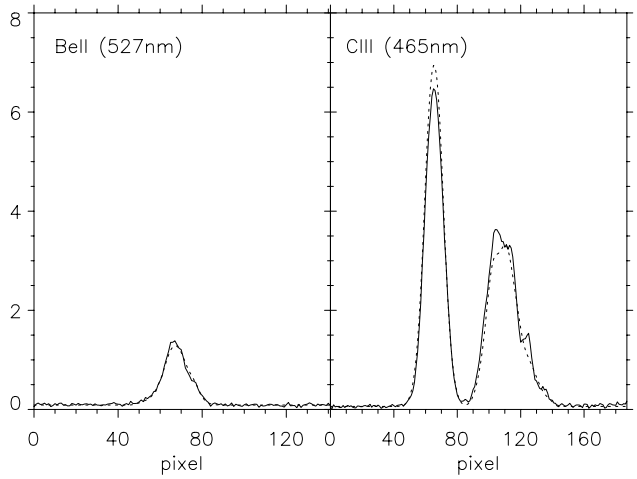

Figure 28: Measured line shape for the BeII and CIII features (solid line) and corresponding fitted modelled spectral line shape (dotted line). The fit is with contributions from the high- and low-field sides of 1:1.3 for CIII and 1:0.5 for BeII.

4.4 Plasma impurities and plasma wall interaction

The second main theme of the research in this thesis has been the development and application of visible spectroscopic diagnostics for information gathering about impurities and plasma wall interaction [69, 70]. This is another significant issue in fusion development and

is the focus of many strands of research. The influx of impurities into a fusion plasma has important implications for the quality of the plasma since radiation from the impurities, in particular from high-Z materials, leads to energy losses (see section 1.1).

Impurities in EXTRAP T2R have been the principal concern of papers I and II. In the former, metallic impurities in the form of Cr, Fe, Mo, Ni and Mn (neutral and singly ionised) along with oxygen and nitrogen impurities are identified from a spectroscopic survey of the visible wavelengths. The metallic impurities indicate there is interaction of the plasma with the stainless steel vessel walls and molybdenum mushroom limiters. It is generally accepted that the oxygen originates from air and water vapour contamination during vacuum breaks and through long term diffusion from small leaks. Oxygen can form oxide layers on the metal surfaces that have been shown to affect the hydrogen recycling (retention and permeation) in the walls [71, 72].

The concentration of the OV and OIV ionisation stages (n_i/n_e) was investigated using the line-of-sight measurements of line radiation, experimental emissivity profiles from paper VIII and PECs with assumed profiles of T_e and n_e. The low concentrations (<1%) over the whole plasma confirm that although oxygen is a major impurity in EXTRAP T2R its levels are not prohibitive for fusion reactions. Calculations of the oxygen ion densities were also carried out in paper VIII following the calculation of the emissivity profiles, in this case for all ionisation stages OII to OV and OVII. Although the corresponding concentrations are slightly less than those in paper I, both papers have the concentration of OV greater than OIV in the central region and this reversed further out. The paper I calculated concentrations were 0.3% and 0.2% for OV and OIV in the core up to ~half radius and 0.6% and 0.7%, respectively, further out.

The remainder of paper I and the whole of paper II are concerned with impurities (and the main gas) in the edge region of the plasma where influx and recycling due to plasma wall interaction is instrumental. Although measurements are made on lines-of-sight through the plasma, the neutral ions, and hence their line radiation originates from the edge regions and the issues of radial profiles of electron temperature and density profiles are less important. Indeed the Balmer line ratio technique described in section 2.4 was used to estimate the local T_e (and n_e) of ~1-5eV and $0.5\text{-}1*10^{12}cm^{-3}$. Note here that the measurements of the different Balmer lines H_α to H_δ were made in separate discharges in a series with the same parameters where the discharges were assumed to be reproducible.

Quantitative calculations of the particle fluxes were made from the measured photon fluxes using the method detailed in section 2.4 in both papers I and II, in the former using fitting of measured spectral line shapes and in the latter using monochromator measurements. The work in paper I concentrates on the relative fluxes of the different ions where steady state levels of hydrogen were determined to be two orders of magnitude greater than those of chromium, which were double those of molybdenum, and where the hydrogen flux was observed to be an order of magnitude larger earlier in the discharge. In contrast, paper II is concerned with the effect of using the RWM active feedback control system (see discussions in section 4.1) on the plasma wall interaction and impurity influx, observing a 40-50% decrease in the discharge averaged Cr and Mo particle flux with feedback applied, see figure 29. The spectroscopy in this case adds to the understanding of how the active feedback stabilisation system works and affects the plasma and how the plasma interacts with the walls causing the impurity influx. Average deposition rate results from collector probes exposed to multiple discharges agree well with the results from the spectroscopic diagnostic.

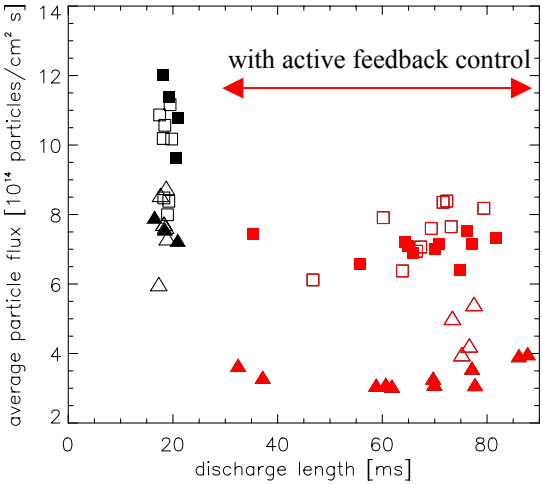

Figure 29: Particle flux results from the spectroscopic diagnostic for molybdenum (Δ) and chromium (□) in H_2 (open symbols) and D_2 (filled symbols) discharges. Discharges longer than 30ms have active feedback control.

The changeover from hydrogen to deuterium main gas is characterised by spectral lines from both ions being present (as shown for the Balmer-α emission line in figure 30). The change in their relative intensity both during each discharge and during successive discharges can shed light on the interaction processes of the plasma with the wall [70] and on the retention and recycling of the main gas. Similar isotopic exchange experiments were previously carried out on the carbon-walled EXTRAP T2 device [73].

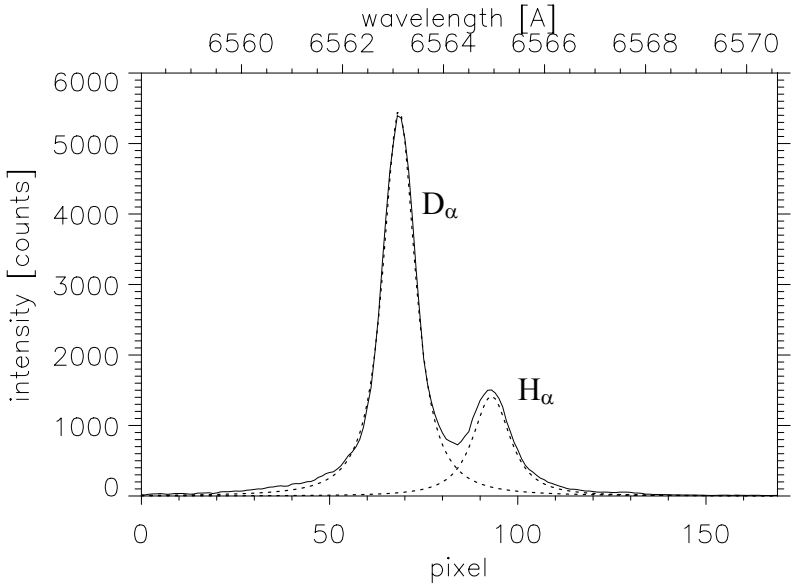

Figure 30: The hydrogen and deuterium components of the Balmer-α line of the EXTRAP T2R plasma, early measurement in first discharge after changeover to a deuterium plasma. The dotted curves show the fitted components.

Paper III is also concerned with the edge region (in this case in the ASDEX Upgrade tokamak divertor) and with interaction with the wall although it is not impurities that are measured. The D_α line intensity is investigated to determine the flux of atomic deuterium (the main gas) and the contribution from the dissociated molecular deuterium, see also sections 3.7 and 4.5. The molecular band radiations in the tokamak divertor of other species, such as CD

or C_2 have also been investigated in both the ASDEX Upgrade and JET tokamaks. As the carbon comes from the wall these and similar species are of interest in terms of the plasma wall interaction and local plasma condition information (e.g. recombining or detached plasma) [74, 75].

4.5 Molecules

Divertor conditions can support the presence of molecules and the molecular deuterium in the ASDEX Upgrade divertor is investigated in paper III. The intensities of the rotational lines in the Q-branches of the v=0-0 and v=1-1 vibrational bands of the D_2 Fulcher band were measured and using the relations in section 2.6 recalculated from the determined T_{rot} without disturbance from interfering lines. The whole band photon intensity was then extrapolated and the molecular particle flux of deuterium calculated (as described in section 2.5) to be of the order $10^{23}m^{-2}s^{-1}$. Results from different lines-of-sight (figure 31) demonstrated an increased flux when the strike point was closer to the line-of-sight and also an increase if the line-of-sight saw the gas puffing. The flux seen by the wide angle line-of-sight, which sees all of the gas puff, is of the same order as direct measurements of the puffing rate from the valve.

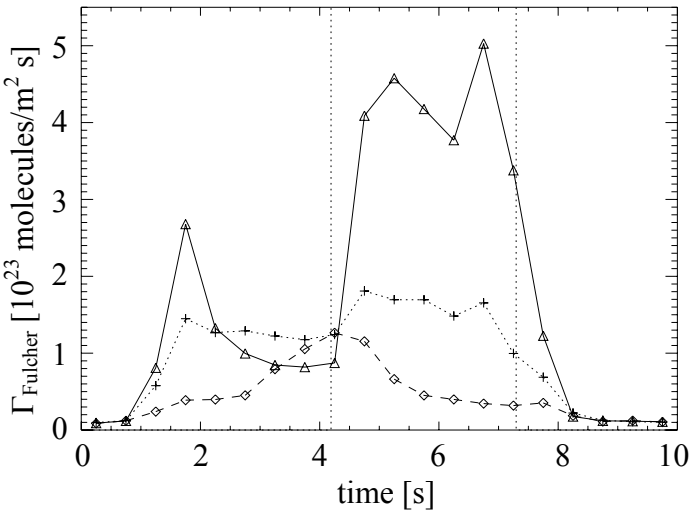

Figure 31: Molecular particle flux calculated from the D_2 Fulcher band measurements in the ASDEX Upgrade divertor. Three lines-of-sight are shown, one wide angle centred on the gas puffing valve (+, dotted curve) and two narrow lines-of-sight one at the valve position (Δ, solid curve) and the other lower down in the divertor (◊, dashed curve). Intensity variations during the flat-top phase (~2-7seconds) are due to the sweeping of the strike point from the initial gas valve position downwards through ~6cm and then back up (turning at ~4.3seconds) and due to the deuterium gas puffing between the two dashed lines [paper III].

An often made naïve assumption is that the D_α line radiation is only atomic in origin, however, dissociated molecules can also contribute. Spectroscopic measurements of the molecular particle flux enabled the contribution from the molecules to the D_α line to be determined. The lines-of-sight further up in the divertor showed a higher contribution of the molecules than those lower down in the divertor with contributions to the D_α of approximately 0.6% and 0.25%, respectively. The level of contribution is approximately constant in the regions above and below the strike point, with a higher molecular contribution

above, so when the strike point is lower down in the divertor, the molecules are more significant to lower positions (for a larger area).

Using the methods outlined in section 2.6 and performing a Boltzmann plot of the measured Q-branch rotational line intensities the upper state rotational temperatures of the v=0-0 and v=1-1 bands were estimated to be a fairly constant value of the order of 1000K. The ground state vibrational temperature was determined at 4000±1000K.

In separate experiments measurements were made of the CD (Gerö) band region to study the changes to the CD band and the overlapping CD^+ band ($A\ ^1\Pi - X\ ^1\Sigma^+$) [76] if present. Figure 32 shows an example of the modelled and measured spectra.

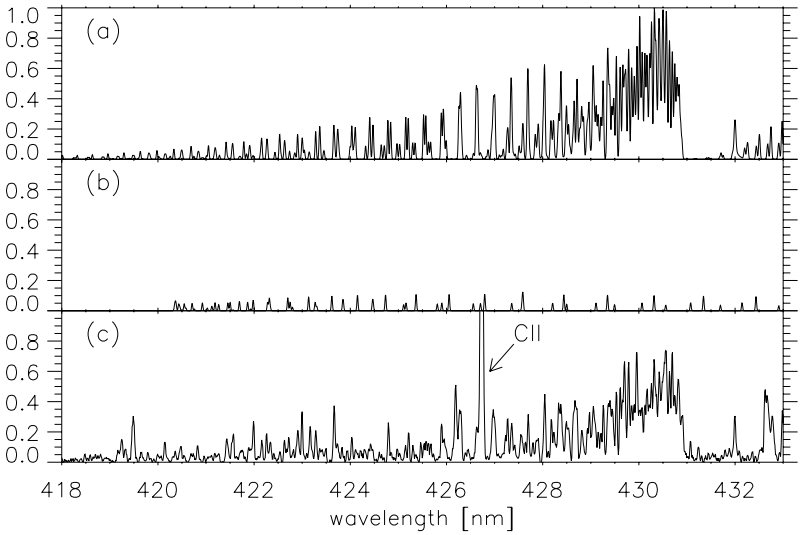

Figure 32: (a) Modelled CD Gerö band ($A\ ^2\Delta - X\ ^2\Pi$); (b) modelled CD^+ band ($A\ ^1\Pi - X\ ^1\Sigma^+$) and (c) corresponding section of the measured spectrum from the ASDEX Upgrade divertor. The intensities of the modelled bands are normalised to lines in their respective band head regions of the experimental spectrum.

4.6 Fluctuations

The small fluctuations and intermittent behaviour of the edge neutral ions were noted before in paper VII where a change (calming) was seen during PPCD (see section 4.2). These irregular fluctuations in the line radiation intensity of the oxygen impurities (including the more centrally located higher ionisation stages) were the primary diagnostic source in paper IX. Here the correlations in the fluctuations observed on different lines-of-sight were successfully used to reconstruct the normalised emissivity profiles of the ions with good agreement to the profiles obtained by the more traditional method of fitting a modelled profile to the experimental data used in paper VIII.

Large periodic fluctuations in the molybdenum (and H_α) intensity are observed in some EXTRAP T2R feedback controlled discharges. These can be correlated with similar fast changes in many of the main plasma parameters such as plasma current, θ, average toroidal field $\langle B_\phi \rangle$, SXR emission and total VUV radiated power, as demonstrated in figure 33. Paper V begins to investigate this global phenomena with the spectroscopy diagnostics, both visible wavelength and beyond, adding to the information and enabling a fuller picture to be gained with the relative timing of the different measurements hinting as to the sequence of events. Whilst the appearance of some of the signals might be reminiscent of a discrete dynamo event

or saw-tooth crash the behaviour of the average toroidal field $<B_\phi>$ is opposite to the typical picture in such cases were a sharp burst (increase) in $<B_\phi>$ followed by a slower decay is seen. Consequently, understanding this observed behaviour is still a work in progress.

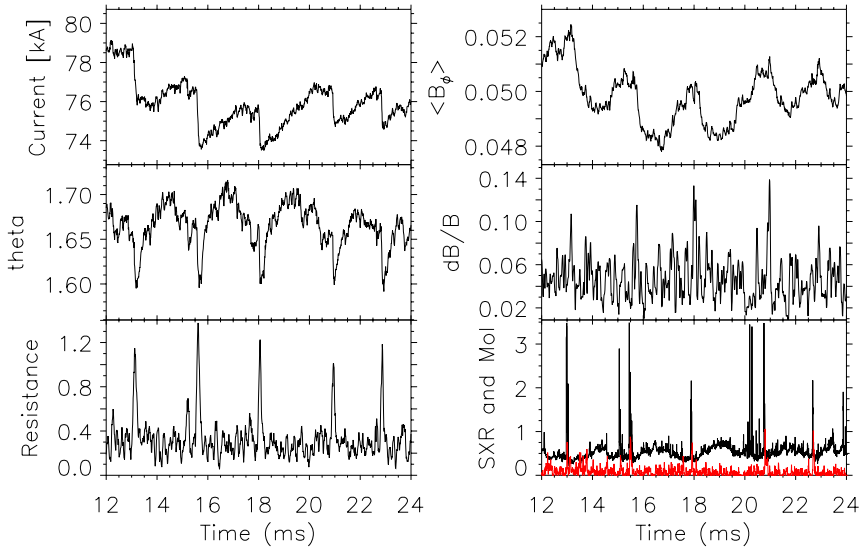

Figure 33: The periodic large fluctuations observed in plasma current (I_p), theta (θ), resistance, average toroidal field $<B_\phi>$, total magnetic fluctuation level dB/B and in last panel SXR intensity (black) and MoI intensity (lighter) [paper V].

5. Summary of papers

5.1 Paper I: Impurity identifications, concentrations and particle fluxes

In this paper a systematic study is made of the visible emission lines from the EXTRAP T2R plasma. Lines originating from various ions (H, O, Fe, Cr, Mo, Ni, Mn, N) and transitions are identified and the some of the different behaviours in time are highlighted. No carbon emission is observed. The concentrations of OIV and OV are calculated from measured line-of-sight spectral line strengths and experimentally determined emissivity profiles and are found to be less than 1% of n_e at all radii and less then 0.5% in the central region. The edge conditions (electron temperature and density) are estimated with the help of the ratio of hydrogen Balmer lines indicating a low T_e of the order 1-5eV at $n_e \sim 10^{12} cm^{-3}$. These values were then utilised with measurements of the neutral ion line radiation to determine the particle fluxes of hydrogen (main gas) and of impurities chromium and molybdenum – of the order $1*10^{16}$, $7*10^{13}$ and $3*10^{13}$ particles/cm^2s, respectively.

Large error bars are quoted in the paper for the metallic ion particle flux calculations. In both the Cr and Mo cases the fluxes are calculated in three separate emission multiplets and an average taken, with the corresponding standard deviation reported. There is a large spread in the fluxes calculated in the separate multiplets (for example 15, 4 and $1*10^{13}$particles/cm^2s for the Cr multiplets), which leads to the large uncertainties given. The differences between the multiplets indicate possible uncertainty in the atomic data or in the intensity calibration.

Previously visible wavelength survey scans have been made of the EXTRAP T2 and EXTRAP T1 plasmas [77]. Significant amounts of carbon, along with oxygen, nitrogen, hydrogen and chlorine, were observed in the plasma of the carbon tiled EXTRAP T2 vessel. All these (including carbon) and additionally Fe, Cr, Mg and Mn were present in the stainless steel EXTRAP T1 which did not have the Mo limiters of the current EXTRAP T2R device.

5.2 Paper II: Impurity influx and plasma wall interaction

In this paper the particle fluxes of metallic ions in EXTRAP T2R are investigated. Two different techniques are used with the average particle fluxes derived from the spectroscopic diagnostic favourably in agreement with those from the collector probes exposed to several discharges. The application of the active feedback control scheme is observed to reduce the average metallic particle flux (reduce the plasma wall interaction). Reductions were of the order 40-60% for Cr and Mo from spectroscopy and Mo and Fe from the probes with a greater reduction seen in D_2 plasmas than in H_2, in particular for Mo probe results. For the spectroscopy, particle flux levels of the order $4.7*10^{14} cm^{-2}s^{-1}$ (with feedback) and

$7.7*10^{14}cm^{-2}s^{-1}$ (without feedback) for molybdenum and for chromium $7.9*10^{14}cm^{-2}s^{-1}$ (with feedback) and $9.1*10^{14}cm^{-2}s^{-1}$ (without feedback) were obtained. Likely causes of the metallic impurities including physical sputtering, evaporation and arcing are discussed.

There were some differences between the probe and spectroscopy results such as no substantial change in the spectroscopic Cr flux reduction between H_2 and D_2. There are several possible reasons for the discrepancies including that the spectroscopy measures the emission from ions in the plasma and only sees the discharge times, the probes measure average deposition fluxes and also see inter-discharge times through multiple discharge exposure. Further investigations might help resolve the issues.

The particle fluxes of Cr and Mo are more than an order of magnitude greater than those quoted in paper I. The difference might be influenced by a number of possible factors. One possibility is the different discharge conditions between the discharges of paper I and the non-feedback controlled H_2 discharges of paper II. The average plasma current in the discharges of paper II was less than that in the 4-5ms measurement interval of the paper I discharges (~70kA compared to ~85kA) although the θ parameter was approximately the same. Additionally, the fluxes in paper II are an average over most of the discharge (from 2ms on) including the end period where the flux rises in these non-feedback discharges. This may increase the average in comparison to the measurements made from 4-5ms in paper I. The difference between the papers may also be due to the assumed T_e (5eV in paper II and 1eV in paper I). Using a value of 5eV for the paper I analysis would bring the average fluxes above those of paper II (~$2*10^{15}$particles/cm^2s). The multiplets also have different T_e dependencies and use of a higher T_e would reduce the difference between the 359nm and 427nm CrI multiplets seen in paper I, the flux from 521nm multiplet is still much lower.

5.3 Paper III: D_α line radiation and molecular D_2 band radiation

Atomic and molecular emission from deuterium in the ASDEX Upgrade outer divertor is extensively studied in this paper. The line radiation from Balmer D_α is employed to relatively calibrate two (high resolution) spectrometers by simultaneous measurements on an interlaced array of lines-of-sight. Subsequently the D_α radiation and two vibrational bands of the molecular D_2 Fulcher band $d\ ^3\Pi_u \rightarrow a\ ^3\Sigma_g^+$ radiation are measured in the outer divertor during a sweep of the strike point and with D_2 gas puffing. From the molecular band spectrum the upper state rotational temperature of ~1000K and ground state vibrational population and vibrational temperature (of 4000K±1000K) were derived and the molecular particle flux calculated. A flux of ~$10^{19}cm^{-2}s^{-1}$ was calculated on the narrow lines-of-sight. The contribution of the molecular D_2 to the Balmer D_α line was estimated to be less than 1% (and a greater effect above the strike point position than below). The time evolution and the effect of the sweep and puffing of the quantities were studied.

The principal limitations in the accuracy of the calculations are due to the uncertainty in the relative calibration and in the assumptions made as to the values of the S/XB and D/XB for the molecular D_2 calculations for the Fulcher band and the D_α line. The assumptions were required as the values were not always available in literature for the conditions (local electron temperature and density) and for deuterium. We also assumed toroidal symmetry to compare D_α and D_2 measurements in different toroidal arrays. It was also assumed that the Fulcher band and D_α emitting regions were at the same location at the edge in order to use Langmuir probe T_e and n_e (for S/XB, D/XB), but this may not be entirely the case [78].

The resolution of the spectrometer used for the D_2 Fulcher band was needed to discern the rotational lines however only a single vibrational band could be captured at once. If one

could measure more (or all) of the molecular band at once one would not have to worry about inter-discharge factors or extrapolating from a few vibrational or rotational bands.

5.4 Paper IV: Rotation of plasma impurity ions and tearing modes

In this paper the toroidal rotation of the oxygen impurity ions in EXTRAP T2R is investigated through the Doppler shift of spectral lines. Measuring on OII to OVI a higher rotation was observed for more central, higher ionisation, ions (up to 40km/s) with all ions showing a ramp up of the toroidal velocity followed by a slowing down phase. With the application of the active feedback (RWM) mode stabilisation scheme a prolongation of the discharge is accompanied by an extension of the higher velocity phase (from around one wall time (6ms) to twice that). Good agreement in the rotation magnitude and evolution is seen between the centremost OVI ion and the m=1, n=-12 most centrally resonant tearing mode at a similar location. Poloidal rotation of OV and its correspondingly located tearing mode are in relative agreement (at ~25-70km/s, though large uncertainty for OV). Using the measurements of the five ions the radial profile of the toroidal ion rotation is modelled by a parabolic profile with an edge reversal.

The magnitude of the impurity ion rotations is greater than in [79, 80] as the analysis programs have been corrected removing the false assumption that the spectrometer was working in second order rather than first. This is also the reason behind the corrected ion temperatures shown in section 3.6 compared to [80].

With the diagnostics available at present on EXTRAP T2R suitable for the spectroscopic measurement of the (impurity) ion rotation velocity and temperature, one major limitation with the obtainable results has been the relatively poor time resolution. The need to collect photons for a given temporal window and then to read-out the detector pixels (even when a small fraction of the available pixels are stored, for example 34 pixels out of 1024) before the next acquisition constrains the repetition rate (to for example ~2ms). It is difficult to relate alterations in the temperature or rotation to fast events, such as the short PPCD pulses, and effectively diagnose the full spectrum of changes to the plasma in response to these types of events. In an effort to improve the time resolution during PPCD experiments attempts were made to scan the measurement settings during successive similar (same) discharges to reduce the gaps between the gate intervals. However, this method is heavily reliant on the discharge conditions (and the line radiation from the ion) being entirely reproducible.

Attempts at understanding how the rotation and ion temperature vary across the plasma (in addition to their temporal variation) are limited by the available instrumentation. Reconstruction of the radial profiles has been carried out through the measurement of the rotation or temperature of multiple ions (emitting in different regions of the plasma, although actually the ions are not in separate regions but have overlapping emission profiles). However, the number of ions and hence the number of locations or radial points is limited. Additionally, as the measurements are made on lines-of-sight then information such as the emissivity profiles must be known (measured) accurately in order to correctly take into account that often the photons are emitted (in different amounts) over a large part of the line-of-sight.

5.5 Paper V: Parameter fluctuations

Here, we explore the extent of some fast transient phenomena observed in some EXTRAP T2R plasmas. The periodic fluctuations observed in the main plasma parameters such as

plasma current, θ, resistance and average toroidal field are observed to extend also to the spectroscopic signal strengths (line intensities) of neutral molybdenum (and hydrogen) and the SXR – and even to the appearance of the VUV spectra (and resulting total radiated power). The periodicity is stable within a discharge at 2-5ms. Through examining the relative timing of the events, the sequence and consequences of the different changes are established. A period of improved conditions with increasing I_p and $<B_\phi>$ is followed by a fast SXR spike, echoed in the MoI, leading to an increase in the plasma resistivity and a sharp drop in I_p, θ and $<B_\phi>$. High ionisation stage impurities then rise in the VUV. The likelihood and magnitude of such events are explored in terms of basic parameters of theta, I_p and discharge length. Further investigation is required to understand the phenomena.

5.6 Paper VI: Active feedback mode control

The effect of the application of the active feedback stabilisation system for the resistive wall modes on a wide variety of plasma parameters is investigated in this paper. From a spectroscopic point of view, variations in the toroidal rotation velocity and ion temperature of the OV ion are examined. Rotation velocities of 30-50km/s are observed after the initial ramp-up phase and ion temperatures of 300-450eV (higher during feedback controlled discharges) are measured. Changes in the intensity of the neutral hydrogen, molybdenum and chromium line radiation and in total radiated power and SXR emission are also observed with the use of active feedback control. Radial profile measurements of the different quantities indicate the regions most affected for the different radiation types. Studies of the time evolution during feedback controlled discharges of the radial profiles of the radiation in different wavelength regions indicate no major transformations but some minor changes in terms of peaking and radial position.

Further investigation of the effect of the active feedback stabilisation on the neutral impurity ions has been carried out in paper II. Measurement of the active feedback stabilisation effect on the rotation and ion temperature of other oxygen ions and not just OV could give a fuller picture of the ion behaviour with information on any profile changes to the ion velocity or temperature adding to the study of changes in the ion emissivity profile in this paper. Improvements in the operation of the active feedback stabilisation schemes continue to be made.

Active feedback stabilisation capabilities have also been installed and operated on the RFX device [61]. Successful suppression of the growth of field perturbations and discharge prolongation with an increase in global energy confinement have been demonstrated. Changes in the electron and ion temperatures are observed.

5.7 Paper VII: Pulsed poloidal current drive effects

The effects of the application of pulsed poloidal current drive (PPCD) on the feedback controlled EXTRAP T2R plasma is investigated in this paper. A reduction in the normal fluctuation activity in the neutral line radiation (impurities Cr and Mo and main species H) during PPCD is observed (with a return to the usual behaviour afterwards) suggesting a change in the edge region and in the plasma wall interaction. In agreement with tearing mode behaviour, no change is seen in the OV toroidal rotation. Some increase in the OV ion temperature may be indicated. Different amplitudes of PPCD are investigated to find the optimum level, detrimental effects are observed with the highest amplitude, including spikes

in the resistive voltage and in the metal impurity influx and early termination. The effect of PPCD on the ion emissivity profiles is investigated in paper VIII.

5.8 Papers VIII and IX: Radial profiling of impurity ions

In these papers measurements of impurity line radiation on an array of five lines-of-sight in EXTRAP T2R are utilised to determine the emissivity and density radial profiles of the ions. The emissivity profiles are determined by fitting the measured data with an assumed asymmetric Gaussian profile in paper VIII and by correlating the small fluctuations in the line integrated intensity measured on the different lines-of-sight in paper IX. Using assumed electron temperature and density profiles absolute ion density profiles are then determined in paper VIII through the photo-emissivity coefficients. Both techniques produce oxygen ions emissivity and density profiles that are broad and overlapping with the higher ionisation stages peaking closer to the centre. The emissivity profiles of the neutral metallic ions of Cr, Fe and Mo are narrower and located closer to the edge. Transport modelling calculations and changes in the OIV and OV density profiles are employed to investigate impurity transport during applied PPCD. Here, reduced transport in the core leads to the observed impurity profile changes in the core whilst the edge effects can be explained by electron temperature changes. Stiff ion density profiles are observed during tearing mode growth after mode-locking in discharges not controlled by active feedback.

6. Conclusions and outlook

This thesis has explored the field of visible spectroscopic diagnostics and their application and development in fusion plasmas. A number of techniques for the measurement and analysis of spectroscopic signals have been described along with the limitations and assumptions and their effects. The benefits of the obtained range of plasma parameters were examined in relation to what they could tell us about the plasma and the discharge scenarios in operation.

We have studied the EXTRAP T2R plasma and discovered what impurity ions are present. The plasma edge and interaction with the surrounding walls and limiters has been investigated through measurements of the neutral impurity and main plasma ions. Analysis has enabled us to estimate edge conditions such as electron temperature and to calculate atomic particle fluxes. We have measured the reduction in influx (and plasma wall interaction) observed when active feedback stabilisation of the resistive wall modes has been used and looked at the time evolution of the flux and how it is affected by pulsed poloidal current drive. Agreement was demonstrated between the particle flux results obtained with spectroscopy and those from collector probe measurements.

Bringing in the higher oxygen impurity ionisation stages and moving away from the edge we have developed and used profile reconstruction techniques to determine the emissivity and ion density radial profiles. The time evolution and effect of feedback and pulsed poloidal current drive on the profiles have also been studied. Measurement and analysis of the spectral line widths and wavelength shifts have yielded ion temperatures and rotation velocities. We have looked at their variation with time and again what effect active feedback control and current drive have. A correlation between tearing mode and ion rotation has been established and we have investigated how the ion temperature and rotation varies over the plasma radius through measurements of multiple ions and radial profile reconstruction.

We have examined radiation in the ASDEX Upgrade and JET tokamak divertors, both line emission and molecular band spectra. Rotational and vibrational temperatures have been extracted through analysis of the molecular band structure and molecular particle fluxes were calculated. The influence of molecular D_2 on the D_α Balmer-line was measured and the effect of varying local conditions observed. Atomic line shape and Zeeman splitting analysis in the JET main plasma was probed for estimation of the emitting ion location.

The development and use of spectroscopic diagnostics informs us about the plasma conditions, both local and global, and about parameters such as particle transport and particle influx. We are able to gain a wider picture of the effect and consequences of actions taken and control schemes applied, it adds to our knowledge, helps us to understand and to successfully operate, improve and develop fusion devices and scenarios towards the future.

It is clear that visible spectroscopic diagnostics play a vital role in the development of fusion. We have the prospect to look forward to of a wide range of these diagnostics being

installed on the next step device ITER, on other new and redeveloped devices and on future machines. It is likely that diagnostics will be less important by the time we come to future reactors, as hopefully we will understand what is going on and only need to monitor conditions for control and safety rather than for the wider range of parameters that currently help us to interpret our experiments. The flexibility of the optical fibre based visible spectroscopy diagnostics coupled with their non-disturbing nature means that they can be good candidates for the real time feedback control loop signals needed for future devices. It is therefore important to continue to develop visible spectroscopic diagnostics.

Abbreviations

a – minor radius
ADAS – Atomic Data and Analysis Structure [40]
A_{ik} – spontaneous radiative emission probability of line A_{ik} and multiplet A_{IK}
ASDEX Upgrade – Axially Symmetric Divertor EXperiment tokamak device in Garching, Germany (see section 1.3)
B_ϕ – toroidal magnetic field, with average toroidal field $\langle B_\phi \rangle$ and poloidal magnetic field B_θ
β – the angle between the line-of-sight and the rotation
CCD – charge coupled device
$\langle \cos\beta \rangle$ – the line-of-sight average of $\cos\beta$ weighted by the measured emissivity profile
DIII-D – (Doublet III-D) graphite tokamak with divertor in San Diego, USA (General Atomics and international collaboration) [81]
EFDA – European Fusion Development Agreement
$\varepsilon_i(r)$ – radial profile of the emissivity of the ion i, with $\varepsilon_i(l)$ for the line-of-sight profile
EXTRAP T2R – (EXTRAP = External ring trap) reversed field pinch in Stockholm, Sweden (see section 1.2)
F – reversal parameter, $F=B_\phi(a)/\langle B_\phi \rangle$, ratio of edge to line averaged toroidal magnetic field
FWHM – full width at half maximum, with experimental ($FWHM_{Expt}$), Doppler ($FWHM_{Doppler}$) and instrumental ($FWHM_{Inst}$) variants
$\Gamma_{particle}$ – particle flux
H_α – hydrogen Balmer-α, with D_α for the deuterium equivalent
I – intensity, with multiplet intensity (I_{IK}, Φ_{photon}) and line intensity (I_{ik}, I_J)
I_p – plasma current
ITER – (International Thermonuclear Experimental Reactor) the next step reactor experiment in Cadarache, France (see section 1.1)
JET – Joint European Torus in Culham, England (see section 1.3)
λ – wavelength, with zero-velocity unshifted wavelength λ_o and shifted wavelength λ_{shift}
LCFS – last closed flux surface
MHD – magneto-hydrodynamics
(m,n) – poloidal and toroidal mode number respectively
MSE – Motional Stark Effect
MST – Madison Symmetric Torus, reversed field pinch in Wisconsin, USA [82]
NBI – neutral beam injection
n_e – electron density, with $\langle n_e \rangle$ for the line averaged electron density
$n_i(r)$ – radial profile of the ion density
n_i/n_e – concentration of the ion with respect to the electron density
OMA – optical multi-channel analyser
OV – the ionisation stage O^{4+} of oxygen (with 4 electrons removed), other ions are given in the text using the same nomenclature
PEC – photo-emissivity coefficient
PMT – photo-multiplier tube
PPCD – pulsed poloidal current drive
P_{rad} – radiated power
QSH – quasi-single helicity
RFP – reversed field pinch
RFX – (Consorzio RFX) reversed field pinch in Padova, Italy [83]
RWM – resistive wall mode
SOL – scrape-off layer

S/XB – ionisations per photon with ionisation rate S, excitation rate X and branching ratio B. For molecules both the ionisations and dissociations per photon are included in D/XB or (S+D)/XB

SXR – soft x-ray

TdeV – Tokamak de Varennes in Québec, Canada (no longer in operation)

T_e – electron temperature

θ – (theta) pinch parameter, $\theta = B_\theta(a)/\langle B_\phi \rangle$, ratio of edge poloidal to line averaged toroidal magnetic field

T_i – ion temperature

TM – tearing mode

T_{rot} – rotational temperature

T_{vib} – vibrational temperature

UV – ultraviolet, with VUV for vacuum ultraviolet

v – velocity, with v_{tor} for toroidal rotation velocity

W_i – statistical weight of line W_i and multiplet W_I

References

[1] HR Griem, *Plasma Spectroscopy*, McGraw-Hill Book Company, New York (1964)
[2] HR Griem, *Principles of Plasma Spectroscopy*, Cambridge University Press, Cambridge (1997)
[3] IH Hutchinson, *Principles of plasma diagnostics*, Cambridge University Press, Cambridge, 2nd Edition (2002)
[4] W Engelhardt, *Spectroscopy in Fusion Plasmas*, Proceedings of the Course: Diagnostics for Fusion Reactor Conditions EUR 8351-I EN (1982)
[5] C De Michelis and M Mattioli, *Rep. Prog. Phys.*, **47** (1984) 1233
[6] T Fujimoto, *Plasma Spectroscopy*, Oxford University Press, Oxford (2004)
[7] A Pospieszczyk, *Transactions of Fusion Science and Technology*, **49**, 2T (2006) 395
[8] E Rebhan and G Van Oost, *Transactions of Fusion Science and Technology*, **49**, 2T (2006) 16
[9] J Wesson, *Tokamaks*, Clarendon Press, Oxford, 3rd Edition (2004) p34
[10] WJ Hogan, *Nucl. Fusion*, **44,** 12 (2004) and papers therein
[11] F Waelbroeck, P Wienhold and J Winter, *J. Nucl. Mater.*, **111-112** (1982) 185
[12] VM Prozesky, *Plasma Phys. Control. Fusion*, **35** (1993) 1717
[13] HAB Bodin, *Nucl. Fusion*, **30** (1990) 1717
[14] SC Prager, *Plasma Phys. Control. Fusion*, **34** (1992) 1895
[15] J Wesson, *Tokamaks*, Clarendon Press, Oxford, 3rd Edition (2004)
[16] *http://www.iter.org/*
[17] AJH Donné, *Nucl. Fusion*, **47** (2007) S337
[18] *http://www.jet.efda.org/*
[19] *http://www.alfvenlab.kth.se/fusion/*
[20] PR Brunsell, H Bergsåker, M Cecconello, JR Drake, RM Gravestijn, A Hedqvist and J-A Malmberg, *Plasma Phys. Control. Fusion*, **43** (2001) 1457
[21] J Sallander, *Time- and space-resolved spectroscopy at the EXTRAP-T2 reversed-field pinch*, PhD Thesis KTH Stockholm (1998) TRITA-FYS-1065, ISSN 0280-316X
[22] *http://www.ipp.mpg.de/ippcms/eng/for/projekte/asdex/index.html*
[23] S Günter *et al.*, *Nucl. Fusion*, **45** (2005) S98
[24] O Gruber for the ASDEX Upgrade Team, *Nucl. Fusion*, **47** (2007) S622
[25] JA Blackburn (editor), *Spectral Analysis: Methods and Techniques*, Marcel Dekker Inc., New York (1970)
[26] AC Lanzafame, DH Brooks and J Lang, *A&A*, **432** (2005) 1063
[27] L Gerö, *Z. Physik*, **117** (1941) 709
[28] NIST Atomic Spectra Database, *http://physics.nist.gov/PhysRefData/ASD/index.html*
[29] CE Moore and JW Gallagher (editor), *Tables of Spectra of Hydrogen, Carbon, Nitrogen, and Oxygen Atoms and Ions*, CRC Press, Boca Raton (1993)
[30] *http://exoplanets.org*
[31] A Hellemans, *Science*, **314** (2006) 1671
[32] L Carraro, ME Puiatti, F Sattin, P Scarin and M Valisa, *Plasma Phys. Control. Fusion*, **40** (1998) 1021
[33] PG Carolan, MJ Forrest, NJ Peacock and DL Trotman, *Plasma Phys. Control. Fusion*, **27** (1985) 1101
[34] J Gafert, W Fundamenski, M Stamp, JD Strachan and contributors to the EFDA-JET workprogramme, *Proc. 28th EPS Conf. on Contr. Fusion and Plasma Phys., Funchal, ECA*, **25A** (2001) 1637

[35] K Krieger, M Stamp, S Brezinsek, HG Esser, S Jachmich, A Kreter, S Menmuir, Ph Mertens, V Philipps and P Sundelin, JET EFDA contributors, *Proc. 34th EPS Conf. on Plasma Phys., Warsaw* (2007) P1.041
[36] JD Hey, M Korten, YT Lie, A Pospieszczyk, D Rusbüldt, B Schweer, B Unterberg, J Wienbeck and E Hintz, *Contrib. Plasma Phys.*, **36** (1996) 583
[37] HR Griem, *Plasma Spectroscopy*, McGraw-Hill Book Company, New York (1964) p101
[38] IH Hutchinson, *Principles of plasma diagnostics*, Cambridge University Press, Cambridge, 2nd Edition (2002) p247
[39] HR Griem, *Principles of Plasma Spectroscopy*, Cambridge University Press, Cambridge (1997) p310
[40] HP Summers, The ADAS User Manual version 2.6 (2004) *http://adas.phys.strath.ac.uk*
[41] S Brezinsek, PT Greenland, Ph Mertens, A Pospieszczyk, D Reiter, U Samm, B Schweer and G Sergienko, *J. Nucl. Mater.*, **313-316** (2003) 967
[42] U Fantz and S Meir, *J. Nucl. Mater.*, **337-339** (2005) 1087
[43] U Fantz, K Behringer, J Gafert, D Coster and ASDEX Upgrade Team, *J. Nucl. Mater.*, **266-269** (1999) 490
[44] GR Möhlmann and FJ de Heer, *Chem. Phys. Lett.*, **43** (1976) 240
[45] S Brezinsek, *et al.*, *Physica Scripta*, **111** (2004) 42
[46] DG Whyte, WP West, R Doerner, NH Brooks, RC Isler, GL Jackson, G Porter, MR Wade and CPC Wong, *J. Nuc. Mater.* **290-293** (2001) 356
[47] U Fantz, B Heger, D Wünderlich, R Pugno and ASDEX Upgrade Team, *J. Nucl. Mater.*, **313-316** (2003) 743
[48] G Herzberg, *Spectra of Diatomic Molelcules*, Van Nostrand, Princeton (1950) p204
[49] U Fantz, *Atomic and molecular emission spectroscopy in low temperature plasmas containing hydrogen and deuterium*, IPP-report **10/21** (2002)
[50] U Fantz and B Heger, *Plasma Phys. Control. Fusion*, **40** (1998) 2023
[51] AJH Donné, *Transactions of Fusion Science and Technology*, **49**, 2T (2006) 349
[52] M Cecconello, *Experimental studies of confinement in the EXTRAP T2 and T2R reversed field pinches*, PhD Thesis KTH Stockholm (2003) ISBN 91-7283-417-X
[53] Y Corre, E Rachlew, M Cecconello, RM Gravestijn, A Hedqvist, B Pégourie, B Schunke and V Stancalie, *Physica Scripta*, **71** (2005) 523
[54] M Kuldkepp, *Diagnostics for advanced fusion plasma scenarios*, PhD Thesis KTH Stockholm (2006) ISBN 91-7178-474-8
[55] IH Hutchinson, *Principles of plasma diagnostics*, Cambridge University Press, Cambridge, 2nd Edition (2002) p141
[56] H Sakakita, D Craig, JK Anderson, TM Biewer, SD Terry, BE Chapman, DJ Den Hartog and SC Prager, *Jpn. J. Appl. Phys.*, **42** (2003) L505
[57] I Condrea, E Haddad, BC Gregory and G Abel, *Phys. Plasmas*, **7** (2000) 3641
[58] LR Baylor, KH Burrell, RJ Groebner, WA Houlberg, DP Ernst, M Murakami and MR Wade, *Phys. Plasmas*, **11** (2004) 3100
[59] JM Noterdaeme, *et al.*, *Nucl. Fusion*, **43** (2003) 274
[60] DJ Den Hartog and D Craig, *Plasma Phys. Control. Fusion*, **42** (2000) L47
[61] S Ortolani and the RFX Team, *Plasma Phys. Control. Fusion*, **48** (2006) B371
[62] K Sasaki, *et al.*, *Plasma Phys. Control. Fusion*, **39** (1997) 333
[63] MS Chu, *et al.*, *Nucl. Fusion*, **43** (2003) 196
[64] PR Brunsell, *et al.*, *Phys. Rev. Lett.*, **93** (2004) 225001
[65] JS Sarff, SA Hokin, H Ji, SC Prager and CR Sovinec, *Phys. Rev. Lett.*, **72** (1994) 3670
[66] Y Yagi, Y Maejima, H Sakakita, Y Hirano, H Koguchi, T Shimada and S Sekine, *Plasma Phys. Control. Fusion*, **44** (2002) 335
[67] DF Escande, *et al.*, *Phys. Rev. Lett.*, **85** (2000) 1662

[68] L Frassinetti, PR Brunsell, JR Drake, S Menmuir, M Cecconello, *Proc. 34th European Physical Society Conf. on Plasma Physics, Warsaw* (2007) P1.115
[69] V Philipps, *Physica Scripta*, **T123B** (2006) 24
[70] G Federici, *et al.*, *Nucl. Fusion*, **41** (2001) 1967
[71] JS Hu, JG Li, XM Wang and YP Zhao, *Fusion Engineering and Design*, **81** (2006) 2175
[72] S Nagata, K Takahiro, *Physica Scripta*, **T94** (2001) 106
[73] D Larsson, H Bergsåker and A Hedqvist, *J. Nucl. Mater.*, **266-269** (1999) 856
[74] S Brezinsek, A Pospieszczyk, MF Stamp, A Meigs, A Kirschner, A Huber, Ph Mertens and JET-EFDA contributors, *J. Nucl. Mater.*, **337-339** (2005) 1058
[75] RC Isler, RJ Colchin, NH Brooks, TE Evans, WP West and DG Whyte, *Phys. Plasmas*, **8** (2001) 4470
[76] Z Bembenek, H Cisak and R Kępa, *J. Phys. B: At. Mol. Phys.*, **20** (1987) 6197
[77] P Hörling, *Applications of visible and VUV spectroscopy at the Extrap-T1 and Extrap-T2 reversed-field pinches*, PhD Thesis KTH Stockholm (1996) TRITA-FYS-1045, ISSN 0280-316X
[78] EM Hollmann, S Brezinsek, NH Brooks, M Groth, S Lisgo, AG McLean, AYu Pigarov and DL Rudakov, *Proc. 32nd EPS Conf. on Plasma Phys., Tarragona, ECA*, **29C** (2005) P4.021
[79] S Menmuir, M Cecconello, M Kuldkepp, E Rachlew, PR Brunsell and JR Drake, *Proc. 32nd EPS Conf. on Plasma Phys., Tarragona, ECA*, **29C** (2005) P4.079
[80] S Menmuir, *Visible spectroscopy as a sensitive diagnostic tool for fusion plasmas*, Licentiate Thesis KTH Stockholm (2005) ISBN 91-7178-222-2
[81] *http://fusion.gat.com/global/DIII-D*
[82] *http://plasma.physics.wisc.edu/mst/index.html*
[83] *http://www.igi.cnr.it/*

Acknowledgements

I would like to take this opportunity to thank all those that have offered me help, support and encouragement whilst I have been engaged in the research work for this thesis and who have contributed in so many ways. Some special mentions are needed.

To Elisabeth Rachlew for giving me the opportunity to come and live in this beautiful city of Stockholm and to do my PhD work in the Atomic and Molecular Physics group at KTH. For all her assistance, encouragement and advice throughout the time that I have spent in Sweden.

A big thanks also to the members of the group, past and present, who have made my time here very enjoyable and who have provided many stimulating discussions and ideas. In particular, Mattias, Gemma, Kasia, Anders, Peter, Emilio and Jesus.

Much of my research has been done with EXTRAP T2R and so thanks also to all those who have been involved in running the experiments, in the data collection and analysis and the discussions. Especially, Per Brunsell, Marco Cecconello, Lorenzo Frassinetti, Dmitriy Yadikin and Henric Bergsåker.

I have also been lucky enough to participate in experiments at ASDEX Upgrade in Germany and therefore thank you to those who have organised, been involved in and helped out there, with a special mention to Ralph Dux, Roberto Pugno, Ursel Fantz and Arne Kallenbach.

Experiments at JET mean that I have come into contact with and been helped by researchers from all over so thanks to all and in particular Sebastijan Brezinsek. My appreciation also to the ADAS group.

And finally, a massive thank you to my parents and the rest of my family. For being there for me with their enthusiasm and support and for all those phone-calls and visits.